HOMOGENIZED RESPONSE OF ULTRA-THIN WOVEN FIBRE COMPOSITES UNDER FLEXURAL LOADING

Nishangani Gowrikanthan

(218078U)

Degree of Master of Science

Department of Civil Engineering

Faculty of Engineering

University of Moratuwa

Sri Lanka

January 2023

HOMOGENIZED RESPONSE OF ULTRA-THIN WOVEN FIBRE COMPOSITES UNDER FLEXURAL LOADING

Nishangani Gowrikanthan

(218078U)

Thesis submitted in partial fulfilment of the requirement for the degree
Master of Science in Civil Engineering

Department of Civil Engineering

Faculty of Engineering

University of Moratuwa

Sri Lanka

January 2023

Declaration of the Candidate and Supervisor

"I declare that this is my own work and this thesis does not incorporate without acknowledgement any material previously submitted for a Degree or Diploma in any other University or institute of higher learning and to the best of my knowledge and belief it does not contain any material previously published or written by another person except where the acknowledgement is made in the text.

Also, I hereby grant to University of Moratuwa the non-exclusive right to reproduce and distribute my thesis, in whole or in part in print, electronic or other medium. I retain the right to use this content in whole or part in future works (such as articles or books).

Signature: UOM Verified Signature Date: 16/01/2023

The above candidate has carried out research for the Masters thesis under my supervision.

Name of the supervisor: Prof. H. M. Y. C. Mallikarachchi

Signature of the supervisor: UOM Verified Signature Date : 16/01/2023

Name of the supervisor: Dr. H. M. S. T. Herath

Signature of the supervisor: UOM Verified Signature Date : 16/01/2023

Acknowledgements

First of all, I would like to express my heartfelt and sincere gratitude to my research supervisors, Prof. Chinthaka Mallikarachchi and Dr. Sumudu Herath, for providing the opportunity to do research under their invaluable guidance throughout. They encouraged and motivated me to do my best. This could not be possible without such good advisors and mentors like them.

I would like to say my special thanks to Prof. Priyan Dias for the valuable comments during the progress reviews which inspired me to think out of the box.

I would love to show my appreciation to Milindu Jayasekara, Nadee Haggalla, Sivananthasarma Lowhikan, and Navaratnarajah Sutharsanan for their support, constructive criticism and helpful discussions.

In addition, I would like to acknowledge all academic staff members of the department of Civil Engineering, for their constant support throughout.

I would like to show my gratitude for the financial assistance provided by the National Research Council, Sri Lanka.

Finally, and most importantly, I am really thankful to my family and friends for their constant source of inspiration and moral support.

Abstract

Design of large space structures is restricted due to the limited storage capacity of launch vehicles. Deployable structures made with ultra-thin woven fibre composites eliminates this bottleneck due to self-deploying nature. These structures can self-deploy using the strain energy stored during elastic folding. Popularity of self-deployable structures got increased due to their high strength, lightweight, and good packaging properties. However, thin woven fibre composites undergo large deformation during folding process due to the formation of high curvature, which causes reduction in bending stiffness. Hence, it is crucial to understand the mechanical behaviour of these structures before implementing, in order to avoid unnecessary failures. Numerical modelling techniques have become popular in this research area due to the advancement of computational methods to obtain the mechanical properties of thin woven fibre composites. Homogenised Kirchhoff plate-based representative unit cell modelling technique with solid elements is considered in this research. Corresponding ABD stiffness matrices are obtained with using virtual work principle, where the repetitive nature of woven fibre composites is represented by periodic boundary conditions.

First, a series of micro-mechanical analyses is carried out to observe the influence of the relative positioning of tows on the mechanical properties of thin woven fibre composites. Various phase shifts between the plies have been considered in this research which might be originated from the inter-ply misalignment during the manufacturing stage. The outcomes of this parametric study clearly depict the variation in in-plane and out-of-plane properties extracted from the ABD stiffness matrices and describe the potential causes for the detected deviations between experimental and numerical results.

Next, a resin embedded unit cell model is developed to predict the non-linear bending behaviour with degree of deformation. Initially, a geometrically linear analysis is carried out and then the analysis is extended to non-linear region to observe the moment-curvature response. Linear analysis results of extensional stiffness and Poisson's ratio showed good agreement with the experimental results extracted from

the literature. However, the out-of-plane properties and shear stiffness values were overpredicted. Similarly, non-linear analysis overpredicted the bending stiffness throughout the considered curvature range. Hence, the resin embedded unit cell model needs further improvements and modifications to accurately predict the out-of-plane properties, and capture the reduction in bending stiffness.

Keywords: woven fibre composites, phase shift, representative unit cell, ABD matrix, non-linear bending behaviour

Table of Contents

List of Figures

List of Tables

List of Abbreviations

Abbreviation	Description
NASA	National Aeronautics and Space Administration
ESA	European Space Agency
MARSIS	Mars Advanced Radar for Subsurface and Ionospheric Sounding
DLR	German centre of aviation and space flight
PBC	Periodic Boundary Conditions
RUC	Representative Unit Cell
FEM	Finite Element Modelling
CLT	Classical Lamination Theory
MPC	Multi Point Constraint
C3D6	Three-dimensional continuum six-node triangular prism elements
C3D8R	Three-dimensional continuum eight-node linear brick elements, reduce integration hourglass control elements
CAD	Computer Aided Drawing
BVP	Boundary Value Problem

List of Symbols

Roman Letters

Symbol	*Description*
1K	Thousand filament tow
A	Cross-sectional area of tow
A	Tow thickness
E_1	Longitudinal stiffness
E_2	Transverse stiffness
E_m	Stiffness of matrix
E_{1f}	*Longitudinal stiffness of the fibre*
E_{2f}	Transverse stiffness of the fibre
G_{12}	Shear stiffness
G_{23}	In-plane shear stiffness
G_{12f}	Shear modulus of the fibre
G_m	Shear modulus of the matrix
M	Out-of-plane moment resultant
N	In-plane force resultants
t	Thickness of the laminate
u	Displacement in the X direction
v	Displacement in the Y direction
V_f	Fibre volume fraction
W	Aerial weight of fabric/film
w	Displacement in the Z direction
Subscripts x,y	In-plane directions of loading
Subscripts 1,2	In-plane directions of material

Greek Letters

Symbol	*Description*
ΔL	Weave length of RUC
γ	Shear stress
κ	Out-of-plane curvature
κ_x	Curvature along the X axis
κ_y	Curvature along the Y axis
κ_{xy}	Twisting curvature
ν_{12}	Poisson's ratio
ν_m	Poisson's ratio of resin
ε	Mid-plane strain
ε_x	Strain in the X direction
ε_y	Strain in the Y direction
σ	Equivalent normal
θ	Rotation

1. INTRODUCTION

1.1. Overview

Storage space of launch vehicles restricts the construction of large space structures where they have far bigger dimensions than the launchers. The idea of deployable structures, on the other hand, enables a large structure to fold into a compact shape for storage and transit and then expand back to the functional configuration. Various type of structures like inflatables, mechanically jointed and motorised structures, and stored energy deployable structures were developed using deployable mechanism. Deployable structures manufactured using ultra-thin woven composite materials can store strain energy during folding, and self-deploy using that stored energy. They become more popular due to high strength to weight ratio, ease of manufacture, and favourable packaging properties. Packaging stage of these structures includes folding into high curvatures, which results in change of mechanical behaviour afterwards compared to the initial stage. Hence, understanding the mechanical behaviour of these structures, is crucial for design optimisation.

1.2. Woven Fibre Composites

A structural unit consists of two or more constituent materials is known as a composite. The macroscopic examination is adequate to identify the components of a composite material. At the same time, materials combined on a microscale or nanoscale like metal alloys are usually identified as macroscopically homogeneous materials rather than composite materials.

Invention of plastic and fibreglass to enhance the strength and rigidity were the milestone in composite history. Then, the combination of plastic polymer and fibreglass produced a phenomenally strong structures with reduced weight. However, the fibres alone cannot withstand longitudinal compression and the mechanical properties in transverse direction are significantly weaker than in longitudinal direction. Hence, a transverse reinforcement is necessary to hold the fibres together. Generally, a binder (matrix) is used as a reinforcement between fibres and the geometric configuration of fibre became more efficient after the reinforcement with matrix. It was the initiation point of fibre reinforced composites (Johnson, Todd,

2018), (Gibson, 2016) and they become very popular over the traditional metal alloys due to their higher strength to weight ratio. fibre composites are now being broadly used in aerospace industry because of their high strength, light weight, increased damage tolerances and easily tailorable material properties.

Various types of fibre reinforced composite lamina are there to fulfil respective requirements in several fields. Such as, unidirectional lamina, Bi-directional lamina, discontinuous fibre lamina and, woven fibre lamina (Twfik, et al., 2016). The woven nature of the woven fibre composite lamina does not allow to separate the layers apart by tearing. Figure 1. shows the schematic diagram of woven fibre composite lamina, where the basic constituents of it is clearly indicated. Tow is the major component in woven fibre composite made of bundle of fibres and resin (matrix) which transfers the load. A particular pattern of tow arrangement is known as ply (lamina).

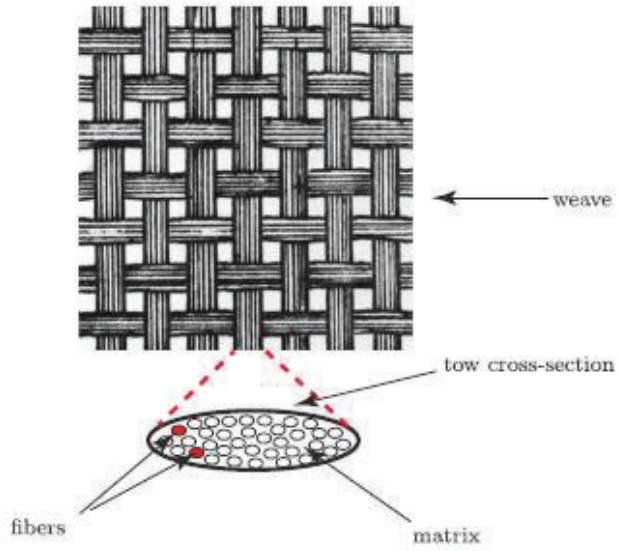

Figure 1.1 Schematic diagram of woven fibre composite (Mallikarachchi, 2019)

Woven fibre composite laminates are more suitable in weight sensitive aerospace applications like solar sails, satellites, star shades and telescopes due to their desirable characteristics. Most importantly, it catches the attention among the other materials due to the self-deploying nature where it can store energy while folding and it uses that stored energy for deployment.

Most of the previously mentioned space structures are comparatively much larger than the payload capacity (weight and volume) of launch vehicle, Figure 1.. Hence, they need to be packed into a compact configuration during transportation and then deployed when necessary. This idea of deployable structures eliminated the bottleneck associated with payload capacity of launch vehicles.

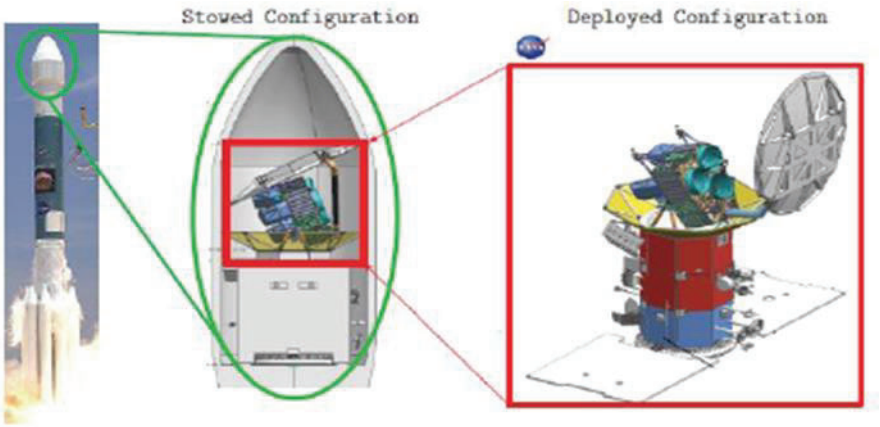

Figure 1.2 Stowage of satellite (source: NASA)

Mechanical hinges were commonly used in designing the deployable structures at early ages (see Figure 1.3). However, due to the heavy weight and complexity in operating these hinges, the idea of self-deployable structures became popular. Where, self-deployable structures store energy while folding and use that stored energy for self-deployment when the calms are released. Hence, elastically deformable materials with high strength to weight ratio is in demand for space applications. Thin woven fibre composites is a good candidate in this regard.

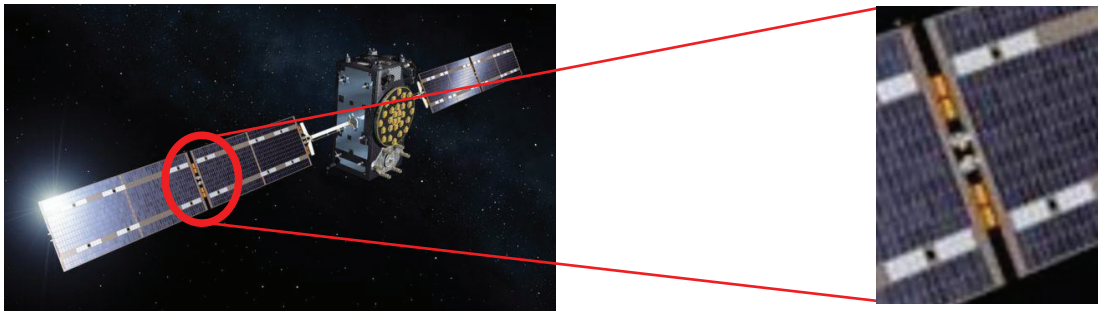

Figure 1.3 Satellite Galileo with mechanical hinges (source: Gunter's Space page)

1.3. Recent Developments and Challenges

Self-deployable structures are used in various space applications focusing on specific mission objectives. Figure 1.4 shows few examples of proposed structures where woven fibre composites are being used.

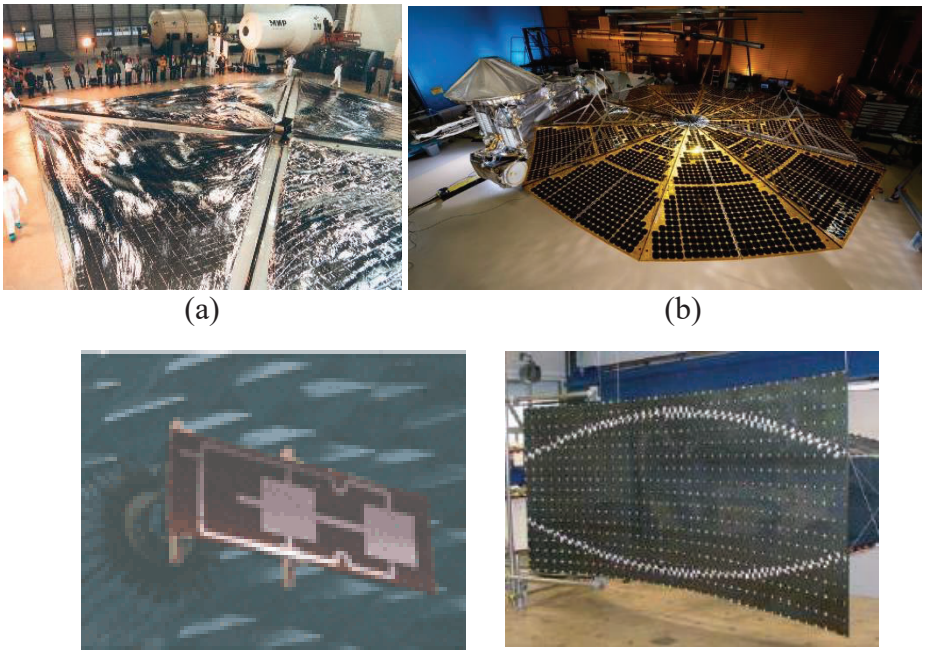

(a) (b)

(c) (d)

Figure 1.4 Self-deployable structures: a) solar sail b) solar array c) antenna d) solid reflectors [source: NASA, Space news.com, (Soykasap, et al., 2008), and (Soykasap, et al., 2004)]

These deployable structures subjected to high curvatures and experience large deformations during both folding into compact configuration and deployment operation. Figure 1.5 shows two examples where space two antenna structures are folded into a highly compact configuration.

Hence, the mechanical properties of woven fibre composites under high curvature should be understand clearly for design optimization. Presently, design improvements are mainly performed through trial-and-error experimental procedures performed on Earth. However, conducting physical experiments under reduced gravity are time consuming, highly expensive and complicated to proceed. Understanding the accurate

behaviour before implementing the project is crucial as demonstrated by the antenna structure with three deployable booms (see Figure 1.6) sent to Mars orbit being failed to deploy after reaching the destination. Therefore, to understand the mechanical behaviour of these deployable structures, the accurate prediction of the mechanical properties of the material used is important.

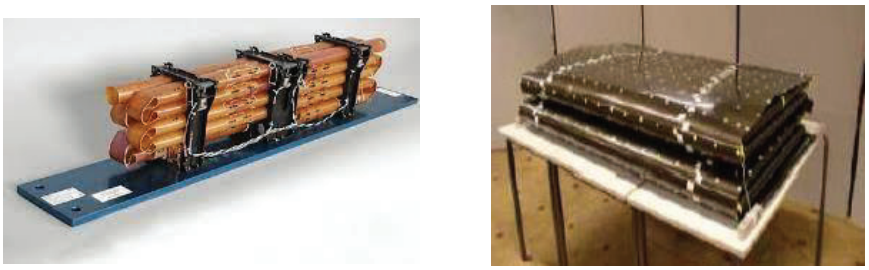

Figure 1.5 High curvature applications (source: European Space Agency and (Soykasap, et al., 2004)

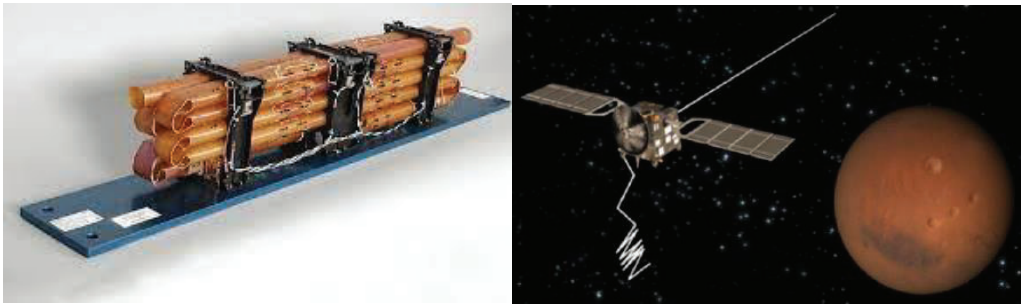

Figure 1.6 MARSIS antenna (source: European Space Agency)

Classical lamination Theory (CLT) is commonly used to calculate the mechanical properties of composite laminates. It yields accurate results for unidirectional fibre composites but, it is not suitable for ultra-thin woven fibre composite laminates due to violation of assumptions of uniform distribution of fibre and constant thickness of the laminate (Jones, 1998, and Soykasap, 2006). Further, CLT does not consider tow waviness and varying thickness which are the basic characteristics of thin woven fibre composite laminates. Although, CLT predicts both in-plane and out of plane properties of woven fibre composite with three or more plies with good accuracy, it over predicts the bending properties of ultra-thin woven fibre composite laminates (single ply and two ply) by 200% - 400% (Soykasap, 2006).

Eventually, numerical modelling techniques have become more popular over physical experiments due to their advanced computational methods and easiness in adopting required material and geometric properties. Hence, these numerical modelling techniques have extensively used in this research area for the accurate prediction of mechanical properties of woven fibre composites. Several studies have been conducted to capture the mechanical properties of woven fibre composites considering various idealisations on some of the key characteristics. Such as, considering different dimensional elements for modelling like, one dimensional element (Cox, et al., 1994, Ichihashi, et al., 1994, Kueh & Pellegrino, 2007, and Hamillage & Mallikarachchi, 2017) or solid elements (Karkkainen & Sankar, 2006, Mallikarachchi, 2019, and Nadarajah, et al., 2019) imposing various interconnections between tows like, separate interface element (Ichihashi, et al., 1994) rigid beam connectors (Soykasap, 2006, and Mallikarachchi, 2019), multi point constraints (Kueh & Pellegrino, 2007), surface based cohesive interaction (Jayasekara, 2020), using several idealized tow cross sections and tow paths like, rectangular or sine curve (Mallikarachchi, 2019) or elliptical cross sections with trapezoidal or sine curve or cubic Bezier (Nadarajah, et al., 2019) tow paths, imposing adhesive material between tows (Mallikarachchi, 2019), various relative positionings of tows like, stacking plies with different rotation phases (Mallikarachchi, 2019), stacking plies with different translation phases (Soykasap, 2006 and Mallikarachchi, 2019).

With the exception of the relative positioning of tows with respect to the translation phase (Fibre configuration), the best idealization for each of the key characteristics has been identified from the aforementioned studies. Fibre configuration is the translation between two plies with respect to one another. There are countless variations of relative positioning. The two extreme fibre configurations with 0° and 180° phase differences are called ‘fibre in-phase’ and ‘fibre out-of-phase’ respectively (see Figure 1.7). The inter-ply slippage of two-ply composites during the manufacturing process produces various fibre configurations in between these extreme cases, which is clearly be seen from the micrograph shown in Figure 1.8. Soykasap (2006) considered the extreme fibre configurations and found that the extreme cases yield upper and lower bounds for the bending stiffness values from the experimental results. Hence, 90° phase difference is considered during my undergraduate research (Nishangani, 2021) and effects of 0°, 90°, and 180° phase shifts on the mechanical properties of thin-woven fibre composites were

analysed. However, variation on the mechanical properties due to the intermediate cases between 0° and 90° angles needs to be studied further to improve the accuracy of the predicted results.

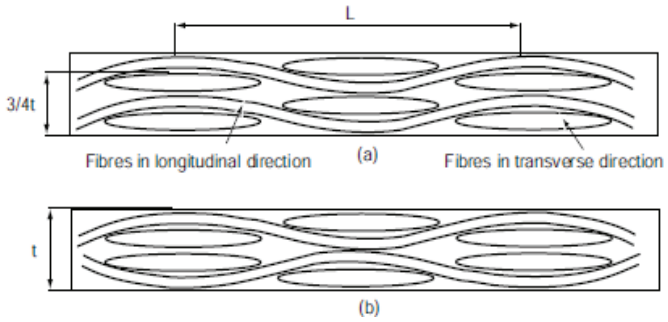

Figure 1.7 Schematic cross section (a) fibre in-phase (b) fibre out-of-phase (Soykasap, 2006)

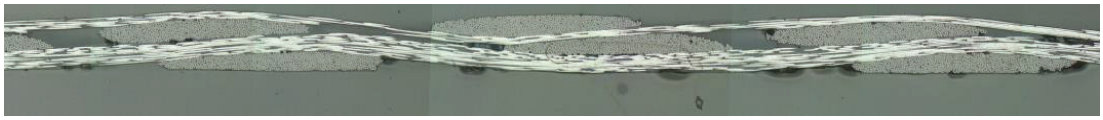

Figure 1.8 Micrograph of two-ply plain weave laminate (Mallikarachchi, 2019)

Most of the aforementioned studies achieved in obtaining the in-plane properties with reasonable accuracy (Kueh & Pellegrino, 2007, Bednarycyk & Arnold, 2003, Kwok & Pellegrino, 2016, Herath & Mallikarachchi, 2016, and Woo & W., 2001). Few number of research studies have captured the bending behaviour of woven fibre composites with a reasonable accuracy (Jayasekara, 2020) which is a governing factor in aero-space applications (Ferreira, et al., 2016, Thomson, 1999, and Mallikarachchi & Pellegrino, 2011). Research studies by Hamillage & Mallikarachchi, (2017), and Jayasekara (2020), well predicted the out-of-plane properties in the linear region (small curvatures). Mallikarachchi, (2019) captured both in-plane and out-of-plane properties in a single model for linear regime.

Experimental studies performed on two-ply plain weave carbon fibre reinforced polymer laminates by Mallikarachchi & Pellegrino (2013) reported a considerable reduction in bending stiffness when subjected to high curvatures while folding (refer Section 2.1.1). Even though the bending response for non-linear region are predicted

with reasonable accuracy in some research studies using numerical models (Hamillage, et al., 2019, and Jayasekara, 2020), the bending behaviour in non-linear region until failure needs to be understood further for design optimisation.

1.4. Research Objective and Scope

As described above, present work on thin woven fibre composites are limited to prediction of material constituent properties under small curvatures and assumes a linear behaviour up to failure in macro models. Further these studies were confined to extreme fibre orientations and did not consider the variation of relative positioning of the tows with respect to each other appropriately.

While the broad aim of this research is focused on developing numerical models for predicting the bending behaviour of thin woven fibre composites under high curvatures, following specific objectives were addressed.

1. Study the effect of varying fibre orientation (relative positioning of fibres with respect to each other) on mechanical properties
2. Predicting nonlinear bending properties under high curvatures considering the effects of variation in fibre-matrix interactions

First the study is focused on capturing the effects of relative positioning of tows on mechanical properties of thin-woven fibre composites. Rather than restricting the analysis to a specific fibre arrangement (one phase angle extracted from the micrograph, Figure 1.8), variation of fibre arrangement is studied by examining six different phase angles.

Development of a numerical model that represents an ultra-thin woven fibre composite laminate to predict the non-linear bending behaviour with degree of deformation was performed on a newly developed resin embedded model. First, the soundness of this model was checked by analysing it in linear regime and then the analysis was extended to nonlinear region.

The majority of space applications prefers single to two-ply laminates due to weight restrictions. This study, therefore places more emphasis on two ply woven laminates. Hence, a two-ply plain weave carbon fibre reinforced polymer laminate made with

T300-1k carbon fibres and HexPly913 resin was considered in this research study. Required geometric parameters of woven fibre composite laminate are obtained from the micrograph, Figure 1.8.

Two different types of Representative Unit Cell models were developed using 3D elements for each objective. The geometry of the model was initially created using finite element pre-processor, TexGen and then imported to Abaqus finite element software as dry fibre models with various tow relative positionings in order to carry out the first part of this research.

Then, the same fibre in-phase model was exported as a resin embedded model in a ".stp" file into 3D modelling software, Fusion 360 and the resin at the mid of the RUC has been removed to replicate the nature of woven fibre composite laminate. Finally, the RUC model was exported as a ".step" file to Abaqus to fully develop the model as described in Section 3.3 to achieve the second objective of this research study. One of the key considerations is having the resin around the tows with voids in appropriate locations and another main consideration is the surface based cohesive interaction between resin and tow surfaces to capture the slipping behaviour between them (Jayasekara, 2020).

Most of the developments carried out in Abaqus finite element software are same for both types of the models considered. The appropriate methods of applying interactions are explained clearly under Section 3.3.3. Necessary reference points and dummy nodes are created in order to apply the required boundary conditions using python code which is elaborated under Section 3.3.1.

Finally, the improved dry fibre RUC models were analysed in the linear region and the effects of phase differences on mechanical properties were examined. The improved resin embedded RUC model was analysed in the linear region ignoring the geometric non-linearity to check the correctness of the model. Then the analysis was expanded as non-linear analysis to capture the non-linear bending behaviour.

1.5.Chapter Organisation

This research thesis consists of 5 chapters. Following the present introductory chapter, Chapter 2 begins with a literature review, explaining self-deployable booms,

multiscale modelling technique, analytical and numerical methods carried out in previous research studies to obtain the mechanical properties of woven fibre composites.

Chapter 3 describes the method followed to develop the numerical model. Beginning with creating the realistic geometric model of a Representative Unit Cell (RUC) of the woven fibre composite using TexGen finite element pre-processor and Fusion 360 3D modelling software incorporating the geometric and material properties and developing the numerical model of the RUC using commercially available finite element software package Abaqus/Standard imposing the appropriate boundary conditions and interactions between the surfaces. Then, explanation on the theory behind the ABD stiffness matrix formulation concludes Chapter 3.

Chapter 4 presents the influence of relative positioning of tows on mechanical properties of ultra-thin woven fibre composites in comparison with the experimental results obtained from the literature.

Chapter 5 presents the non-linear moment-curvature relationship of thin woven fibre composites obtained from the non-linear analysis and comparison of the results with the experimental results available in the literature.

Chapter 5 concludes the research thesis with necessary recommendations for future works.

2. LITERATURE REVIEW

This chapter reviews the latest literature on self-deployable thin walled tubular booms, and the necessity of understanding the mechanical behaviour of ultra-thin woven fibre composite laminates on designing self-deployable booms. Usefulness of multiscale modelling technique in predicting mechanical properties of woven fibre composites is explained and recent developments on analytical and numerical methods are presented.

2.1. Self-deployable Booms

The most frequently utilised deployable mechanism for aerospace structures is self-deployable booms because of the light weight and durability. Due to its capacity to store energy while folding and use that strain energy for self-deployment eliminates the requirement for motorised mechanical hinges. Therefore, the concept of self-deployable structures has allowed the aerospace industry to create cutting-edge designs by overcoming the limited payload capacity available on launch vehicles. Generally, these self-deployable booms are used in various space structures such as, astro-mesh reflectors, solar arrays, and solar sails (see Figure 2.1).

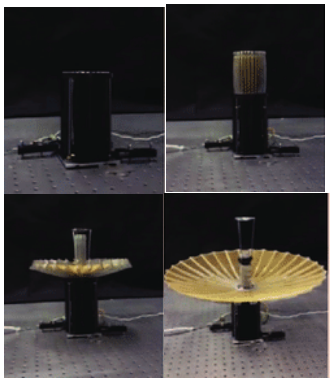

(a) Mesh reflector antennas (Chahat, et al., 2017)

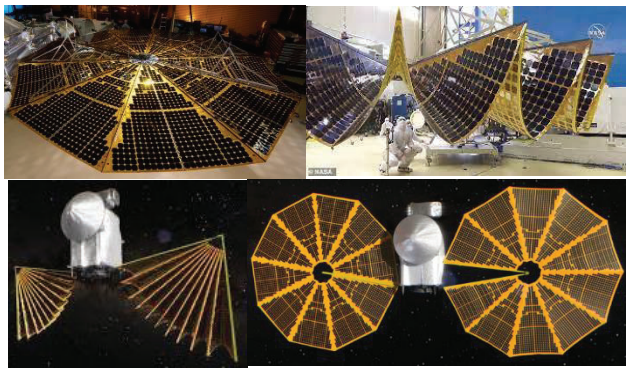

(b) Solar array 'Lucy' (source: (Foust, n.d.))

(b) Solar sail (source: *DLR*)

Figure 2.1 Space structures with self-deployable booms

There are several varieties of booms, including articulated trusses, telescopic tube masts (see Figure 2.2 (a)), coilable masts (see Figure 2.2 (b)), and thin-walled tubular booms. These structures are made of varieties of materials in accordance mission requirements. Although metal alloys were used to produce simple self-deployable structures like carpenter tapes in the past, most of them are now manufactured using woven fibre reinforced polymer composites because of their higher strength, stiffness, and adaptability.

(a) (b)

Figure 2.2 Deployable masts: (a) telescopic tube mast (b) coilable mast (source: (Grumman, n.d.) and (*NASA*))

Tubular booms with thin walls experience extreme curvatures while folding, which can cause high stress and may lead to even failure of the structure. Introduction of longer slotted holes in tubular booms allows certain parts of the structure to operate as tape springs and hence enabling to absorb large deflections as shown in Figure 2.3 (a) (Mallikarachchi & Pellegrino, 2008).

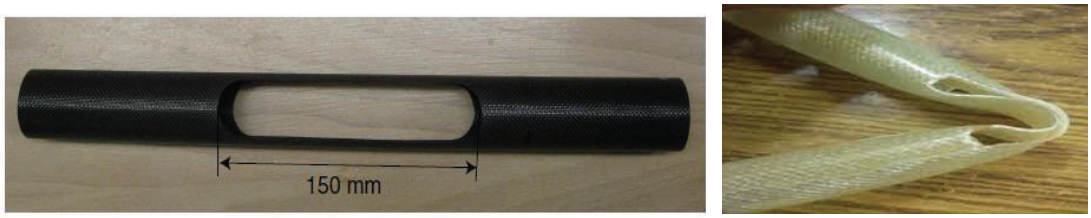

Figure 2.3 Thin-walled tubular boom with slotted holes (a) carbon fibre boom with epoxy matrix (Mallikarachchi & Pellegrino, 2008) (b) glass fibre boom with dual matrix (Swetha Lakshmi, et al., 2022)

Use of dual matrix composite boom which replaced the slotted holes by designing the hinge region with softer matrix (e.g. Silicone) and epoxy matrix in the other parts of

the boom enhanced the level of compaction that can be reached (Ubamanyu & Mallikarachchi, 2016), Figure 2.4.

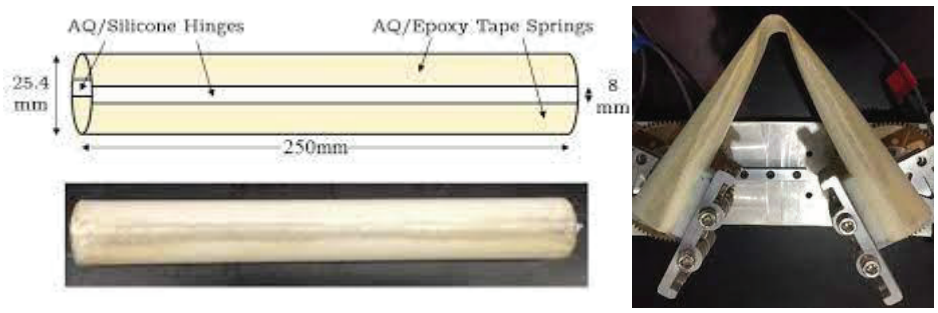

Figure 2.4 Dual matrix composite boom (Sakovsky, et al., 2016)

Numerous simulations have been performed to model the folding behaviour of these boom type structures, and they were successful in capturing the mechanical response (Mallikarachchi & Pellegrino, 2008, Ubamanyu & Mallikarachchi, 2016, and Wijesuriya, et al., 2018). Although, the moment rotation response was not accurately predicted in comparison with the experimental findings because of the usage of constant bending stiffness throughout in simulations (Wijesuriya, et al., 2018). Therefore, exact moment rotation response prediction is essential for the optimization of these booms for aerospace applications.

2.1.1. Experimental Observations

Mallikarachchi (2019) performed a series of experiments on two-ply T300-1k/Hexcel 913 plain weave laminate to obtain the properties. Tensile test, compression test, shear test, bending test, twisting test, and biaxial test were carried out. As mentioned under section 2.1, bending response of ultra-thin woven fibre composite is crucial in aerospace applications. Hence our main focus is on obtaining the moment curvature response. At the same time, tensile response is also taken into account in order to compare and check the applicability of the proposed finite element unit cell models under linear analysis. Tensile response for two-ply T300-1k/Hexcel 913 plain weave laminate is shown in Figure 2.5. The axial stiffness values which are obtained from the tensile test was used under section 4.2.1 for the validation purposes.

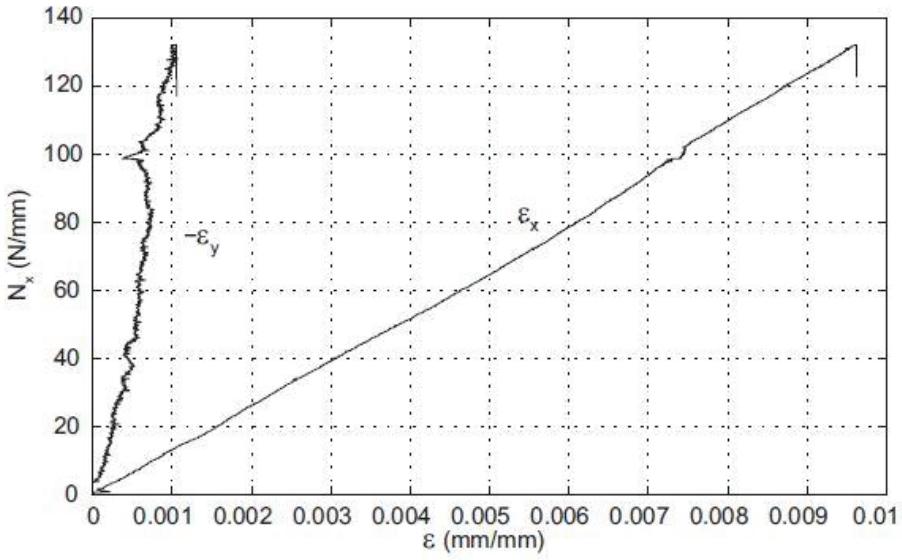

Figure 2.5 Tensile response of two-ply T300-1k/Hexcel 913 plain weave laminate (Mallikarachchi, 2019)

The moment curvature response for a two-ply plain weave CFRP laminate up to a curvature of 0.01 mm^{-1} was obtained through a four-point bending test was performed by (Mallikarachchi, 2019), Figure 2.6 (a). It should be noted that four-point bending test is preferred over three-point bending because the region between two loading point in four-point bending is subjected to a consistent bending moment and hence results are more reliable. The initial bending stiffness was characterized by considering mean and standard deviation of 10 test results considering both loading and unloading. The results indicated that the mean bending stiffness is 37.55 Nmm with a standard deviation of ± 5.54 Nmm. However, this test is not suitable for thin laminates under high curvature, because of large elastic deformation range. Hence, platen folding test, Figure 2.6(b) was performed by (Mallikarachchi & Pellegrino, 2013) and the curvature (κ_x) at failure was obtained by measuring the distance between the two platens (δ) as described by Equation *(2. 1)* The corresponding bending moment, M_x can be calculated using Equation *(2. 2)* proposed by Sanford, et al. (2010) where P denotes force just before the failure and w denotes the sample width.

$$\kappa_x = \frac{2.3963}{\delta} \qquad (2.\ 1)$$

$$M_x = \frac{0.8346\, P\delta}{w} \qquad (2.\ 2)$$

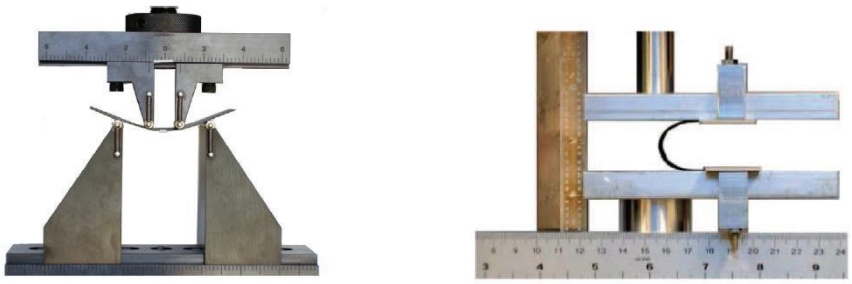

(a) (b)

Figure 2.6 (a) Four-point bending test (b) Platen folding test (Mallikarachchi, 2019)

Seven samples were considered in this experiment and the failure occurred at a curvature of 0.203 ± 0.01 mm^{-1} and the corresponding failure moment was 5.068 ± 0.293 Nmm/mm. However, when extrapolated the initial bending stiffness obtained from four-point bending test, it shows a much higher value of 7.623 Nmm/mm at failure curvature of 0.203 mm^{-1} (see Figure 2.7). Therefore, optimisation of space structures cannot rely on the initial linear stiffness predictions.

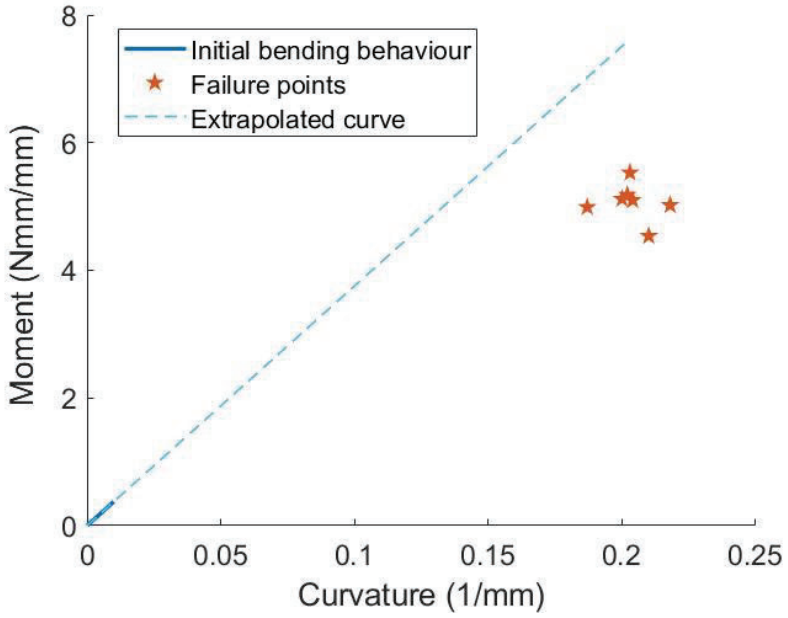

Figure 2.7 Results obtained from four-point bending test and platen folding test (Mallikarachchi, 2019 and Mallikarachchi & Pellegrino, 2013)

2.2. Multiscale Modelling Approach

Multiscale modelling is an approach where several models at various scales are used simultaneously to explain a behaviour of a system. The multiscale modelling approach has been demonstrated to be a potential tool that minimises required experimental testing, hence simplifying design processes and significantly lowering associated expenses (Múgica, et al., 2019). Behaviour of a deployable boom can be considered at several length scales. Dimensionally, these scales are distinguished by the fibre diameter, layer thickness, and laminate thickness respectively and are placed in a hierarchical order as depicted in Figure 2.8. Hence, multiscale modelling technique is embraced in simulation of composite structures made of fibre composites (Ferreira, et al., 2016, Mao, et al., 2013, and Múgica, et al., 2019). The behaviour of the composite boom can be accurately described using an iterative approach that involves continuously updating the bending stiffness at macro-scale (deployable boom) by running the micro-scale simulation (structure of the woven material) simultaneously. The constituent of the boom is constantly being updated with the findings of the analysis regarding displacement and rotation of the boom's deformed shape as described in Figure 2.9. Hence, developing a model to predict the bending stiffness variation accurately is the starting point of this multiscale modelling process.

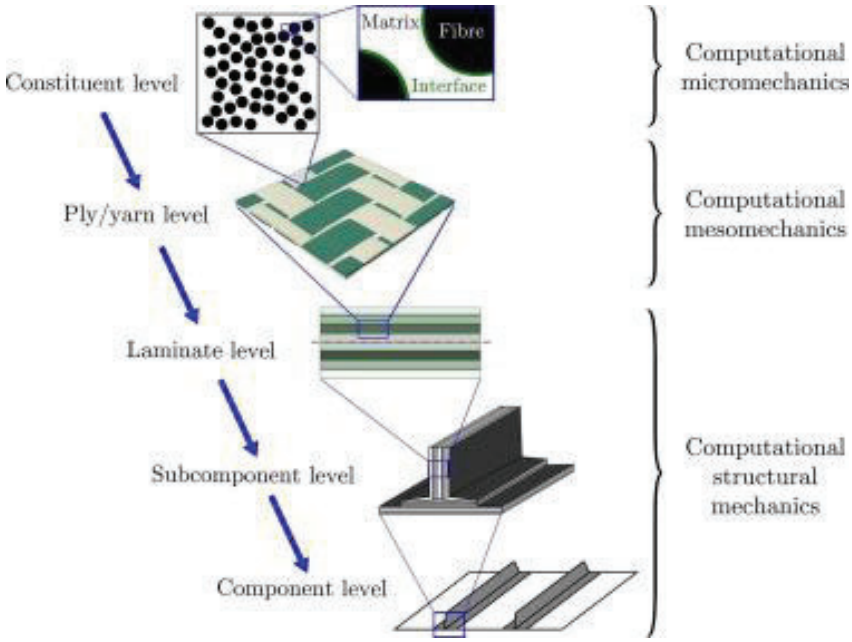

Figure 2.8 Stages of multiscale modelling technique (Múgica, et al., 2019)

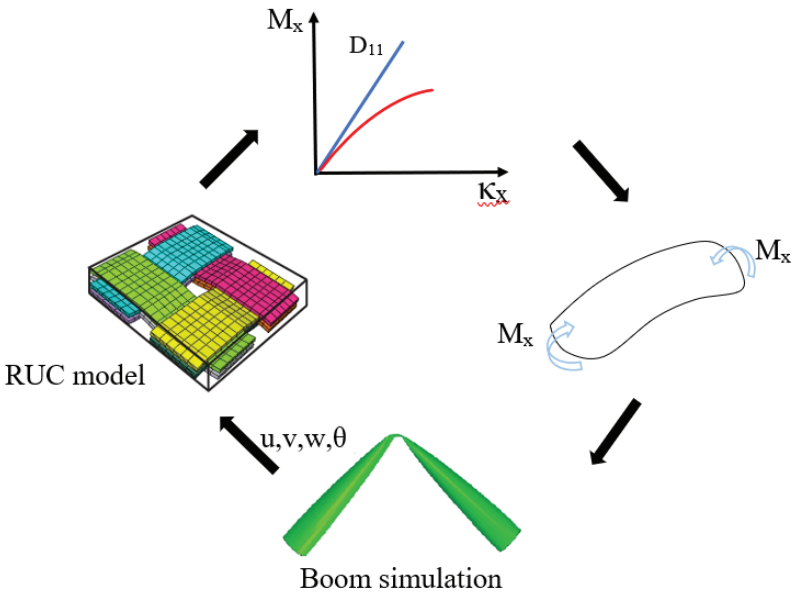

Figure 2.9 Multiscale modelling approach (Jayasekara, 2020)

2.3. Predicting Mechanical Properties

Obtaining mechanical properties of thin woven fibre composites is the amin focus of this research study. Various analytical methods and numerical modelling techniques have been used to predict the mechanical properties in the past. The popular analytical method used in finding the properties of laminated composites is the Classical amination Theory.

2.3.1. Analytical Methods – Classical Lamination Theory

The CLT is a frequently utilized prediction technique that can calculate the strain, displacement, and curvature develop in a laminate. CLT is based on the Kirchhoff-Love hypothesis for shells, which holds that a two-dimensional representation of a three-dimensional plate may be made using the mid-surface plane of the plate. The constitutive relationship between kinematic variables (in-plane strains and curvatures) and static variables (in-plane forces and moments) is first expressed through the analysis of each individual lamina. Equation *(2. 3)* depicts the relationship between stress and strain. Here, $\bar{Q}$ denotes the reduced stiffness.

$$\{\sigma\}_k = [\overline{Q}]_k \{\varepsilon\}_k \qquad (2.\ 3)$$

By integrating stresses throughout each lamina thickness, the final force and moments on a laminate are determined (Jones, 1998).

$$N_x = \int_{-t/2}^{t/2} \sigma_x \, dz \qquad (2.\ 4)$$

$$M_x = \int_{-t/2}^{t/2} \sigma_x \, z \, dz \qquad (2.\ 5)$$

where, N_x is the force applied per unit width of the laminate's cross section, and M_x is the moment applied per unit width, as shown in Figure 2.10. The principal directions of the laminate are indicated here by the letters *x* and *y*.

The fundamental equation *(2. 6)* of CLT is thus found by applying Equations *(2. 3)*, *(2. 4)*, and *(2. 5)*. which yields a 6 × 6 ABD stiffness matrix.

$$\begin{pmatrix} N \\ M \end{pmatrix} = \begin{bmatrix} A & B \\ B & D \end{bmatrix} \begin{pmatrix} \varepsilon \\ \kappa \end{pmatrix} \qquad (2.\ 6)$$

where, $[A]_{3x3}$ sub matrix stands for extensional stiffness matrix, $[B]_{3x3}$ sub matrix stands for extension-bending coupling matrix, $[D]_{3x3}$ sub matrix denotes bending stiffness matrix, ε stands for mid-plane strain, and κ denotes mid-plane curvature. A pictorial description of ABD stiffness matrix is shown in Figure 2.11.

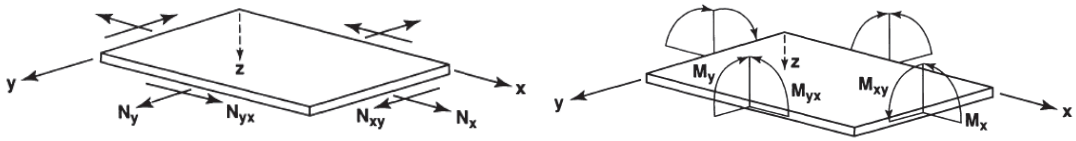

Figure 2.10 In-plane forces and moments on a laminate (Jones, 1998)

However, due to the symmetric, balanced and orthotropic nature of plain-woven laminates, ABD matrix can be simplified with fewer unknown entries as given in Equation *(2. 7)*.

$$\begin{Bmatrix} N_x \\ N_y \\ N_{xy} \\ M_x \\ M_y \\ M_{xy} \end{Bmatrix} = \begin{bmatrix} A_{11} & A_{12} & 0 & 0 & 0 & 0 \\ A_{12} & A_{11} & 0 & 0 & 0 & 0 \\ 0 & 0 & A_{66} & 0 & 0 & 0 \\ 0 & 0 & 0 & D_{11} & D_{12} & 0 \\ 0 & 0 & 0 & D_{12} & D_{11} & 0 \\ 0 & 0 & 0 & 0 & 0 & D_{66} \end{bmatrix} \begin{Bmatrix} \varepsilon_x \\ \varepsilon_y \\ \varepsilon_{xy} \\ \kappa_x \\ \kappa_y \\ \kappa_{xy} \end{Bmatrix} \qquad (2.\ 7)$$

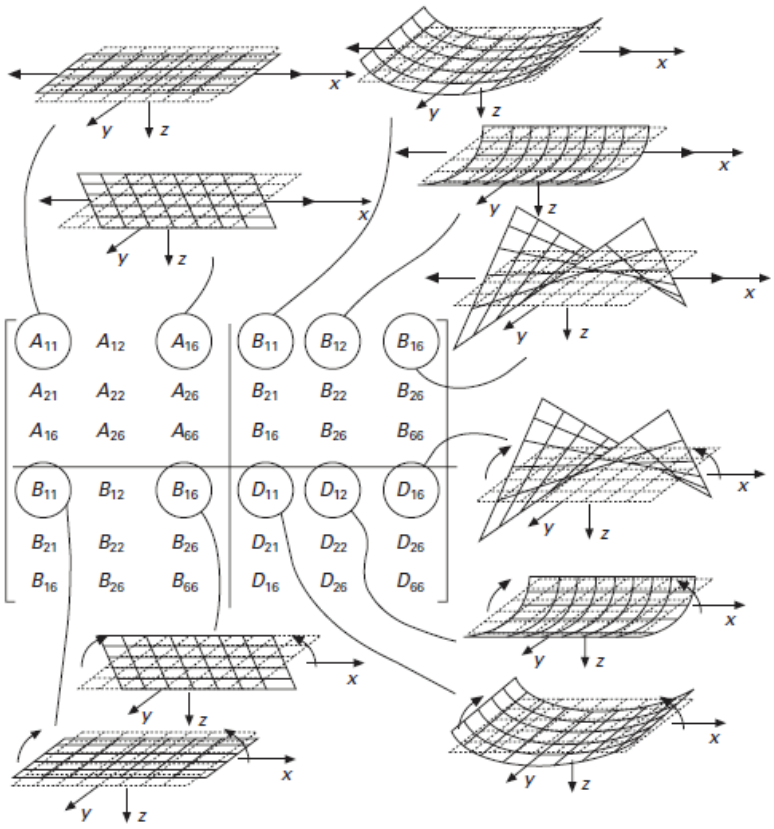

Figure 2.11 ABD stiffness matrix and mechanical deformation for in-plane and flexural loading (Jones, 1998)

The key presumption of the CLT is that, even when the laminate is stretched or bent, the plane sections remain plane and remain perpendicular to the middle surface. This indicates that there should be no shear forces perpendicular to the middle surface (through thickness). It also assumes that the bonds are infinitesimally thin, non-shear deformable, the distribution of fibres and matrix is uniform, and thickness of each lamina is constant. However, most of the aforementioned assumptions are not suitable for thin woven fibre composite laminates. That is because of the tow waviness, varying thickness due to the woven nature (see Figure 1.8), and uneven distribution of fibres cannot be ignored when the number of laminae used in the laminate. As highlighted by Equations *(2. 4)* and *(2. 5)*, laminate thickness plays a vital role in calculating the ABD stiffness matrix. However, CLT provides accurate predictions for laminates with three or more laminas (Soykasap, 2006) because, higher the thickness the lower the variation in thickness as a percentage. Soykasap (2006) stated that, the in-plane properties of thin laminates can be predicted with reasonable accuracy using CLT but,

the out-of-plane properties shows a large deviation up to 200 – 400 % compared to the experimental investigations performed by (Yee & Pellegrino, 2005). This emphasis the necessity of accurate prediction of out-of-plane properties via numerical modelling techniques.

2.3.2. Numerical Modelling of Woven Fibre Composites

Numerical modelling techniques are widely used over physical experiments due to ability of advanced computational tools to adopt the necessary geometrical and material properties and perform virtual simulations at a rapid rate. Meso-mechanical modelling has been widely utilized to precisely estimate the mechanical behaviour of woven fibre composites, which takes into account for the accurate analysis of macroscopic behaviour. Basic steps followed in meso-mechanical modelling technique is depicted in Figure 2.12.

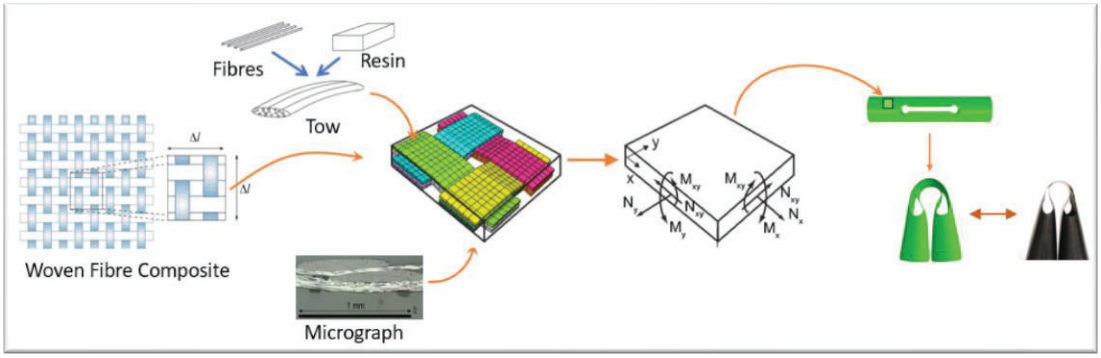

Figure 2.12 Stages of meso-mechanical modelling techniques

An element in the macro model (boom) has been idealised as a homogenised shell element, where Representative Unit Cell (RUC) approach was utilized to model the microscopic behaviour by applying periodic boundary conditions to the RUC. Here, the RUC is a small identical unit in a laminate that can represent the behaviour of actual laminate. RUC was selected considering the repetitive nature of woven fibre composites. The tow and ply arrangement determine the selection of RUC (see Figure 2.13). After selecting the RUC, the appropriate geometric properties obtained from micrographs (see Figure 1.8) and material properties of tows are incorporated into the RUC model. Finally, by analysing the RUC, the stiffness values are obtained. Several

research studies have been carried out to idealise the RUC to replicate the mechanical behaviour

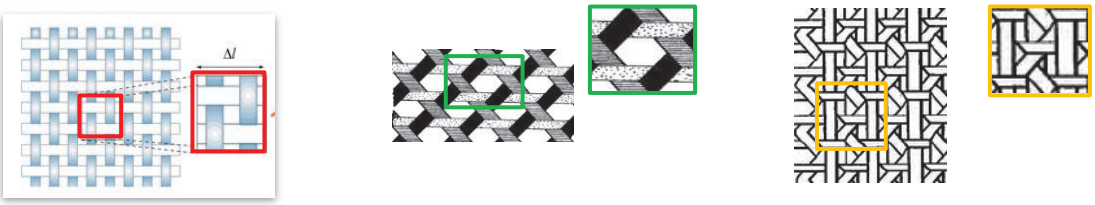

(a) Plain weave (b) Triaxial weave (c) Quart-axial weave

Figure 2.13 RUCs in different types of woven textiles (Soykasap, 2006, and Bilisik, 2012)

Usage of various dimensional elements to model an RUC, several types of inter connection between tows, different idealisations on cross sectional shapes and weave paths, introduction of adhesive materials in between tows, and different ply alignments have been observed in various research studies.

Cox et al. (1994) created a binary model of a 3D composite, Figure 2.14. In this case, the three-dimensional composite was resolved into two basic components: "reinforcing tows" to represent the axial characteristics of individual tows, and "effective medium" to reflect all other properties. This analysis made good estimations about the spatial distribution of tow failures but not produced a detailed stress results in the RUC.

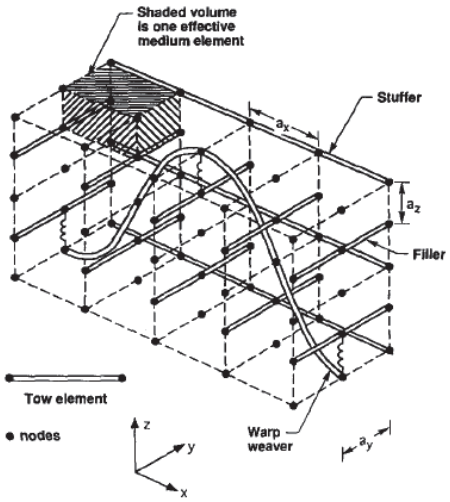

Figure 2.14 Binary model of a 3D composite (Cox, et al., 1994)

In order to estimate the mechanical properties of single ply woven fabric composites, Ichihashi et al. (1994) presented a finite element model utilizing two parallel beam elements incorporating separate interphase element was used to replicate the interconnection between tows (see Figure 2.15) and predicted that the lower modulus and higher strength interphase had a higher resistance to micro fracture.

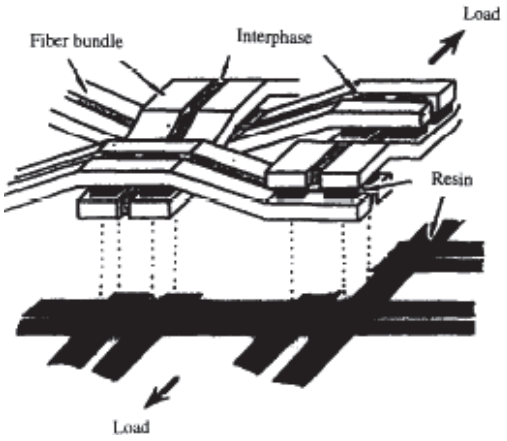

Figure 2.15 Schematic diagram of a single ply woven lamina (Ichihashi, et al., 1994)

Woo et al. (2001) studied the influence of phase shifts on the effective properties of a plain weave composite laminate and considered a low degree of homogeneity where they focused mainly on elastic modulus, shear modulus and Poisson's ratio. Identification of unit cells and application of periodic boundary conditions were done through periodicity vectors. Using microelement mesh and sub meshes, random phase shifts were generated. Woo et al. (2001) observed that, the coefficient of variations (CV) were ranged from 4.5% to 1.5% for elastic modulus and the CV for shear modulus was 0.1%. Hence, it was concluded that there is a significant effect on elastic modulus, and Poisson's ratio and negligible effects on shear modulus due to the phase shifts.

Soykasap (2005) presented micromechanical model using curved beam elements as tows (see Figure 2.17) to predict bending behaviour of woven laminates and resin interfaces at the tow cross over locations are represented by rigid beam connectors. One, two and three-ply woven composites were investigated, and single ply finite element results were predicted accurately with only 3% deviation. However, when

compared to the experimental data, CLT overestimates the bending stiffness of single ply lamina and two-ply woven laminate by 390% and 82% respectively. In addition to that, Soykasap (2005) concluded that, relative positioning of tows plays a major role in bending behaviour of the two-ply laminates. Two extreme fibre configurations (see Figure 1.7) were considered and it was found that they yield the upper and lower bound for the bending stiffness value of the experiment results. Hence, it is evident that the mechanical behaviour of two-ply laminates is clearly influenced by the relative positioning of the tows. So, further investigation on the intermediate phases is necessary for a complete analysis.

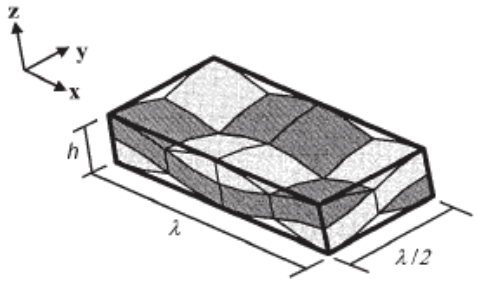

Figure 2.16 Half plain weave unit cell (Woo & Suh, 2001)

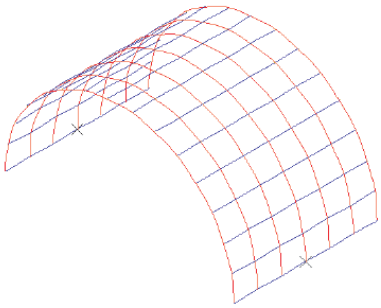

Figure 2.17 Micromechanical model of a single ply (Soykasap, 2006)

Using the RUC created with three-dimensional volumetric elements, Karkkainen and Sankar (2006) established a direct micromechanics approach for investigation of failure initiation of plain weave textile composites to obtain the stress gradient effects (see Figure 2.18). Kirchhoff-love plate theory was used for shells for homogenization where it addresses the bending effects for the first time. The continuum nature of

woven fibre composite was represented by periodic boundary conditions, and the constitutive relationship was produced as an ABD stiffness matrix.

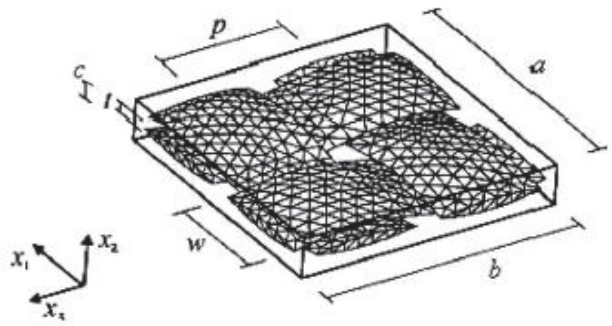

Figure 2.18 RUC of plain weave composite laminate (Karkkainen & Sankar, 2006)

Kueh, and Pellegrino (2007) developed an RUC for triaxial weave laminate using one dimensional Beam elements to obtain the mechanical properties (see Figure 2.19) and applied Multi Point Constraints (MPC) at the tow cross over points to connect them but the relative movement between tows were restricted due to this. The deviation between the predicted and measured values of axial, bending, and shear stiffnesses are 2.9%, 6.4%, and 15% respectively. Hence, it is stated that the stiffness values of single ply triaxial weave fibre composites were predicted with reasonably good accuracy.

Even though, the RUC with beam elements predicted the bending stiffness correctly but it poorly predicts the axial stiffness and Poisson's effects in the case of plane weave laminates. Hence, Mallikarachchi (2019) developed a RUC of two-ply plain weave composite laminate with solid elements to predict the stiffness values. Various cross-sectional shapes and tow paths were considered to check the accuracy of the models (see Figure 2.20). In addition to that a set of reference points were generated at the RUC boundaries and connected to the boundary nodes using rigid beam connectors. The two-ply woven fibre laminate used for the experiment had a fibre volume fraction of 0.62 and hence the volume fraction of the dry fibre model had to be increased to accommodate the additional resin introduced to maintain the connectivity between plies (see Figure 2.20(d)). Application of tie constraints across the whole width of tow provided finer attachment between tow contact regions. The predicted linear analysis results for the unit cell models of the extreme fibre configurations showed deviations with the experimental results less than 7% and 10% for axial and bending stiffnesses respectively.

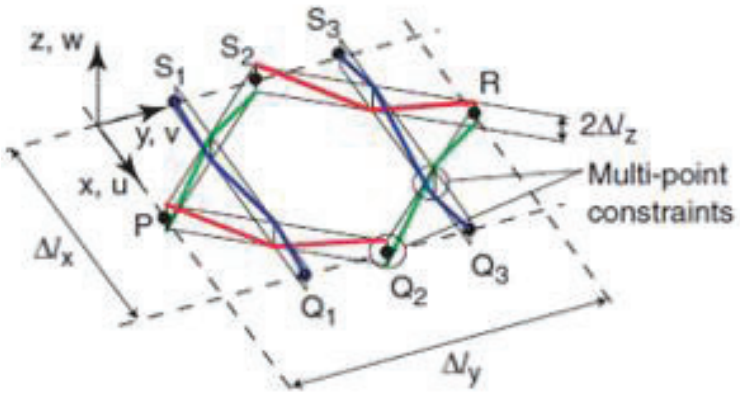

Figure 2.19 Triaxial weave RUC with 1D beam elements (Kueh & Pellegrino, 2007)

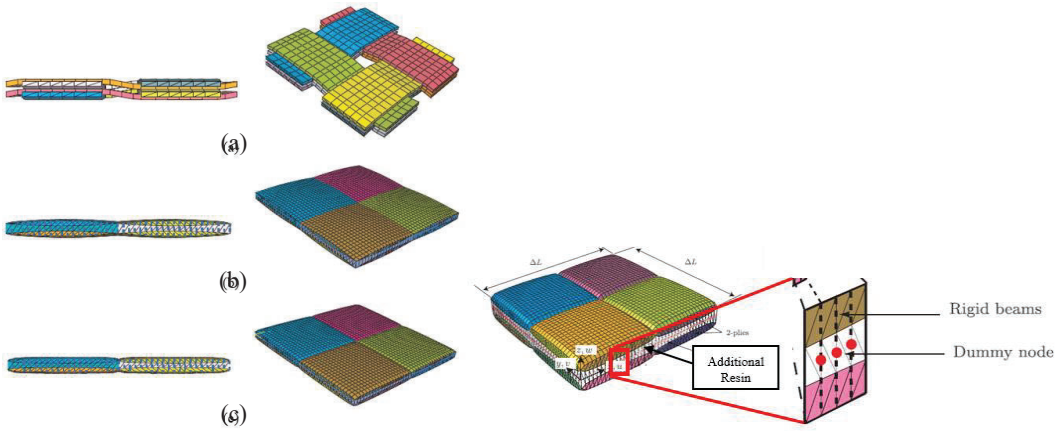

(d)

Figure 2.20 (a) Rectangular (b) Sine curve (c) 4th root of sine curve (d) RUC with additional resin (Mallikarachchi, 2019)

A 1-dimensional beam element model (see Figure 2.21) was developed by Yapa and Mallikarachchi (2017) to predict the non-linear bending behaviour of two-ply plain weave laminates. The model predicted a higher initial bending stiffness with a 21% difference with respect to the mean bending stiffness value obtained from the experiment. However, it captured the reduction in bending stiffness, which is about 23% but it could not be able to capture the non-linearity in bending response until failure point observed from the experiment.

Nadarajah, et al. (2019) proposed a RUC with 3-dimesional solid elements with a suitable tow path named cubic Bezier spline curve (see Figure 2.21). It predicted the

both axial and bending properties with a deviation around 20% in linear region compared to the experimental results but did not capture the correct non-linear bending response.

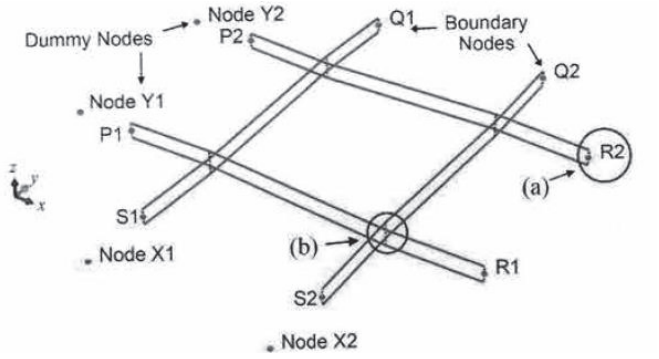

Figure 2.21 1 D beam element RUC model (Hamillage & Mallikarachchi, 2017)

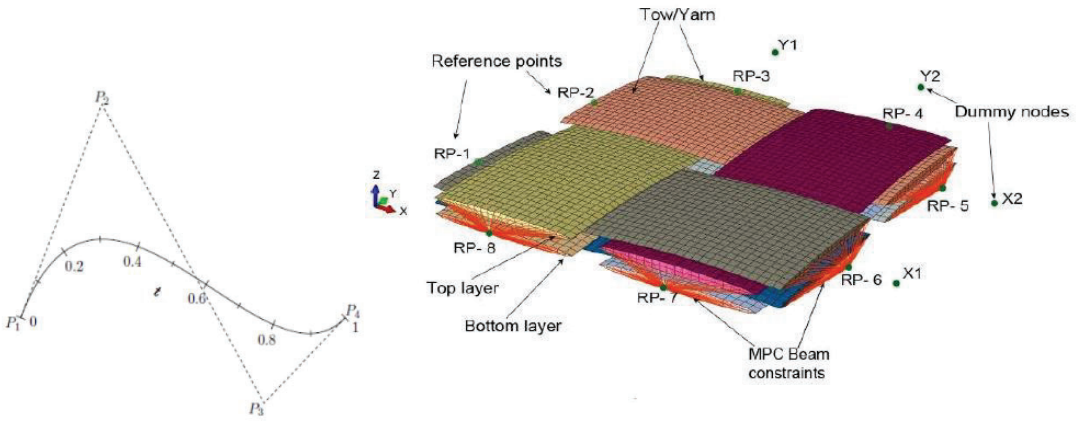

Figure 2.22 RUC with cubic Bezier spline curve as tow path (Nadarajah, et al., 2019)

Jayasekara (2020) proposed RUCs with solid elements as dry fibre model and resin embedded model (see Figure 2.23) and introduced cohesive interactions to allow small sliding between tow to replicate the actuate nature. Dry fibre models were able to predict the non-linear bending behaviour up to a curvature of $0.12mm^{-1}$. However, it underpredicted the in-plane properties of woven fibre composites by 38%. Resin embedded models overpredicted predicted the in-plane properties with a small deviation of 4%, but the bending stiffness value was over predicted by 46%.

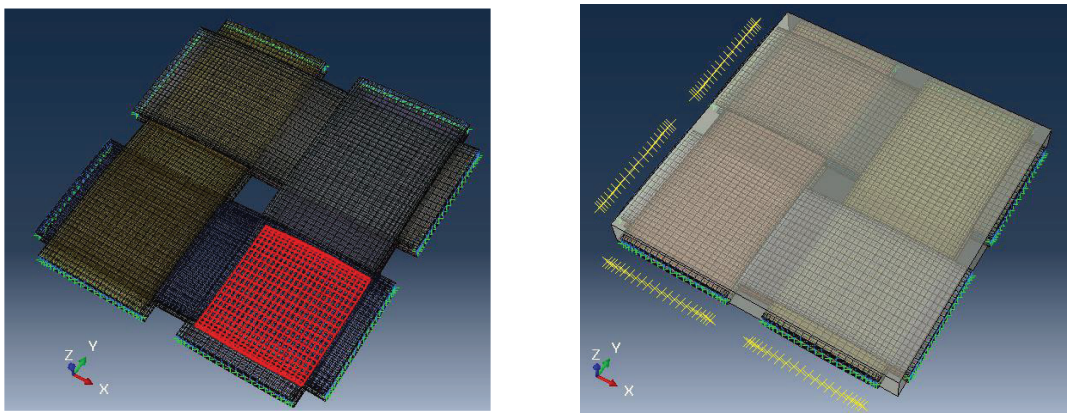

(a) (b)

Figure 2.23 RUC used by (Jayasekara, 2020) (a) Dry fibre model (b) Resin embedded model

In comparison with dry fibre model, the resin embedded model replicates the actual nature of woven fibre composites because the experiment specimen considered in the study (Mallikarachchi, 2011) was manufactured in a controlled conditions with a prespecified resin volume to impregnate the plain weave fabric. This resin impregnation fills the gap between the top and bottom plies and creates a resin layer on top and bottom of the laminate. Predictions can be further improved by considering some unaccounted characteristics in resin embedded model such as interactions between tow and resin, voids in the resin region. Further, a proper investigation on non-linear bending behaviour of the resin embedded model is crucial for future designs.

3. NUMERICAL MODELLING OF A REPRESENTATIVE UNIT CELL (RUC)

This chapter explains the methodology followed in developing the numerical model in performing multiscale modelling that is shown in the Figure 3.1. Starting with the development of the geometric model of a woven carbon fibre composite RUC using a finite element pre-processor, TexGen and a 3D modelling software, Fusion 360 incorporating the geometric properties. Then, development of the numerical model of the RUC using commercially available finite element software package Abaqus/Standard imposing the material properties, appropriate boundary conditions and interactions between the surfaces. Finally, the virtual work theory behind the ABD stiffness matrix formulation to extract the mechanical properties of woven fibre composite is described.

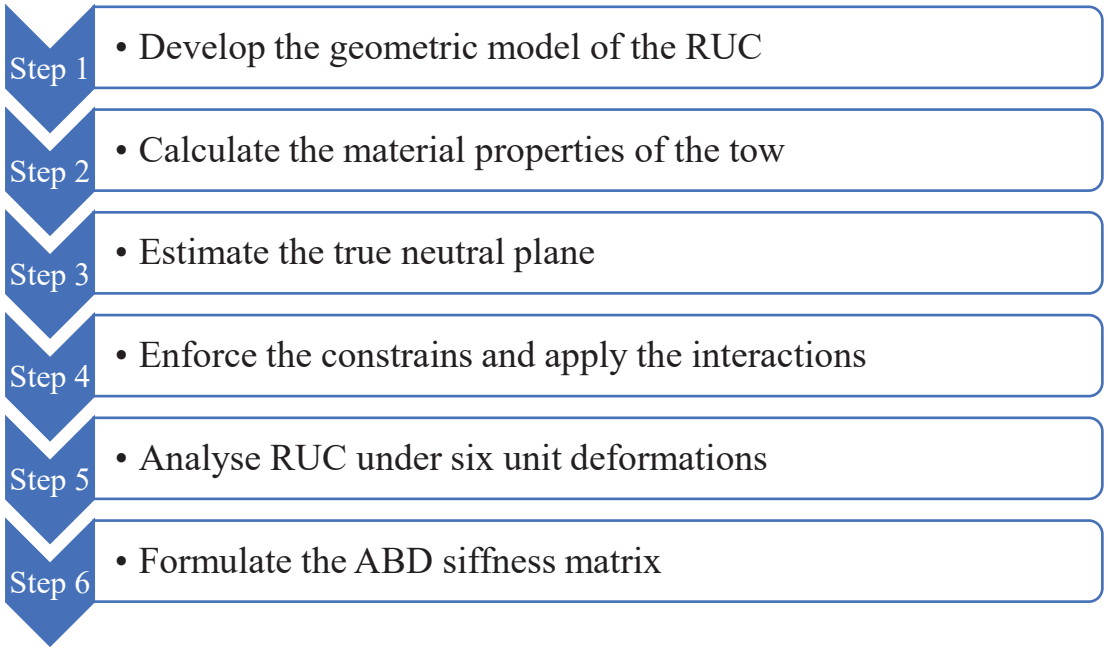

Figure 3.1 Flow diagram of the methodology followed in the numerical modelling of RUC

3.1. Development of the Geometric Model of RUC

The major steps followed in developing the numerical model of RUC is outlined under Section 2.3.2. The initial steps include the selection of suitable representative unit cell

for modelling considering the repetitive nature of woven fibre composite. This selection is mainly depending on the weaving pattern of each ply and ply arrangement in the laminate. Research on effect of various RUC resolution on mechanical properties concluded that, the smaller size RUC predicts the mechanical properties with reasonable accuracy compared to others (Nishangani, et al., 2022). Since, this research study considers a two-ply plain weave laminate, the RUC was selected as shown in Figure 3.2.

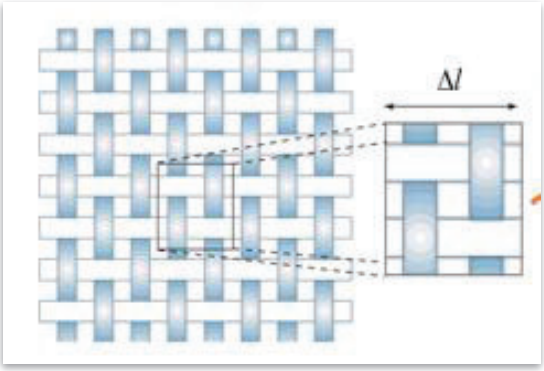

Figure 3.2 Selection of RUC in a two-ply plain weave laminate;
$\Delta l = weave\ length$ (Soykasap, 2006)

3.1.1. Geometric Properties

Geometric properties; such as tow weave length, tow cross sectional shape, tow cross sectional area and tow thickness were extracted from the micrograph (see Figure 1.8) of two-ply plain weave composite laminate made of 1K/T300 carbon fibre and HexPly 913 epoxy resin Mallikarachchi (2019). The actual cross section is changing throughout the weave path. However, the cross-sectional shape was idealised as an elliptical section with a power of 0.5 as stated as the best fit for this micrograph by Jayasekara (2020). Hence, the tow width was found as 1.013 mm. In a study conducted by Nadarajah, et al. (2019), a cubic Bezier Spline curve was determined to be a tow path that was well-suited, and the side length of RUC was taken to be equal to the weave length (2.664 mm). The extracted properties from the micrograph and the calculated properties according to the assumed shape and tow path are tabulated in Table 3.1.

Table 3.1 Geometric properties of 1K/T300/913 two-ply plain-woven composite laminate (Mallikarachchi, 2019, and Jayasekara, 2020)

Geometric property with unit	**Value**
Weave length in mm	2.664
Length along the tow in mm	2.785
Maximum tow thickness in mm	0.059
Tow cross-sectional area in mm^2	0.0522
Tow width in mm	1.013

3.1.2. RUC Geometry Using TexGen

Using the geometric properties collected from Section 3.1.1, the RUC geometry was generated using finite element pre-processor called 'TexGen' (TexGen, 2018), which a textile modelling software. The extracted tow path, weave length and tow cross section details are fed into this software and created the basic geometry of the RUC model. Created geometry can be exported as different types of RUC models with respect to the aims of the research studies. This research considers two different types of RUC models, such as dry fibre model and resin embedded model where, dry fibre model will not have any additional resin around the tows but resin embedded model will have excess resin around the tows.

3.1.2.1.Dry Fibre Model of RUC

Series of dry fibre models are created in order to analyse the influence of relative positioning of tows on the mechanical properties of thin woven fibre composites. As mentioned in section 1.3, in addition to fibre in-phase (0°), fibre out-of-phase (180°) and the 90° shifted RUC model, three additional phase shifted RUC models were generated within 0° to 90°. Initially, an RUC model with fibre in-phase (0°) configuration (see Figure 3.3 (a)) was created and then by shifting the top ply in both x and y directions by three different angles such as 30°, 45°, and 60° other three RUC models (see Figure 3.3) were generated. Any tow misalignments other than phase differences were not taken into account in this study. In addition, unequal phase

differences in the x and y directions, the suggested numerical methods of analysis can be used directly.

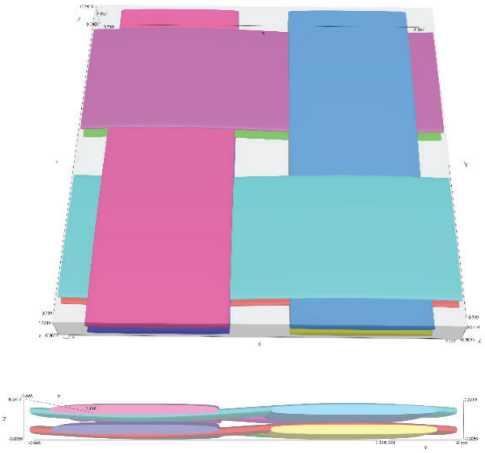

(a) Fibre in-phase configuration RUC model (0°)

(b) 30° shifted in both directions

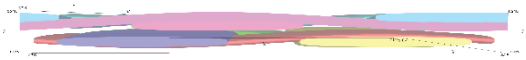

(c) 45° shifted in both direction

(d) 60° shifted in both directions

Figure 3.3 RUC models considered in this study

Then, using pre-developed Python code, each tow is mesh in longitudinal direction with 80 divisions, transverse direction with 28 divisions, and 4 divisions through thickness. In this research, the number of mesh divisions is raised to achieve better results in comparison to earlier studies (Nadarajah, et al., 2019), and (Jayasekara, 2020). The hourglass effect will be eliminated by the finer mesh, which will enable accurate capture of the exact deformation. Finally, these RUC models were exported as dry fibre models to ABAQUS finite element modelling software for the completion of the model. The imported unit cell models are shown in Figure 3.4.

(a) (b) (c)

Figure 3.4 Abaqus Finite element unit cell models of (a) 30° (b) 45° (c) 60° degrees

3.1.2.2.Resin Embedded Model of RUC

Fibre in-phase configuration with zero phase difference between the plies was considered in this part of the research. The generated RUC model was exported from TexGen textile modelling software as a resin embedded model (see Figure 3.5) incorporating the ‘subtracted yarn’ option, so that the tow holes are created into the surrounded resin and finally, the resin embedded RUC model was exported as a STP file to Fusion 360 .

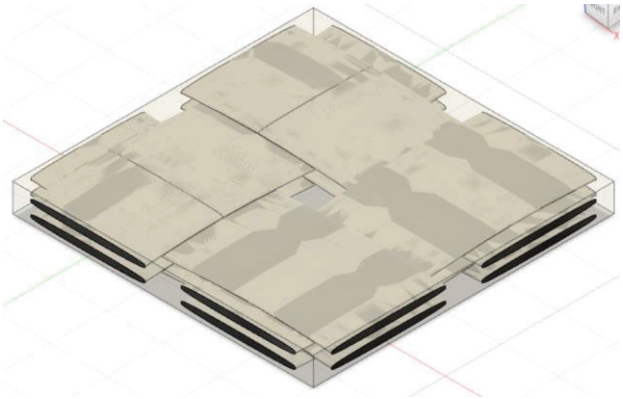

Figure 3.5 Resin embedded model

Resin void found at the mid part of the RUC was added to the imported resin embedded RUC model using push/pull function in Fusion 360 CAD software as shown in Figure 3.6. Then, the modified Resin embedded RUC model was exported as STEP file, so that it can be imported to commercially available Abaqus finite element modelling software to finalise the model development.

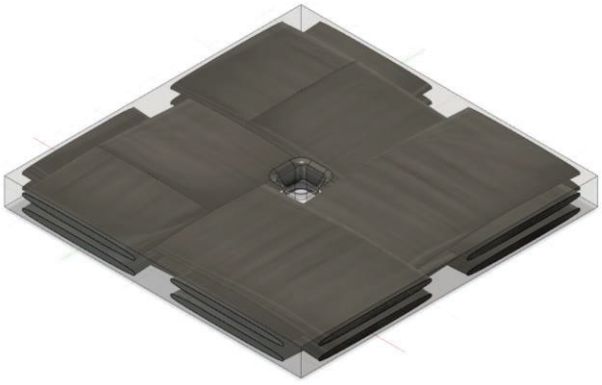

Figure 3.6 Geometrically finalised resin embedded RUC model

3.2. Material Properties of Tow

Tows, the major component in transferring the axial load in the considered composite, is made of T300-1k carbon fibres and HexPly 913 epoxy resin. The material properties of these fibres and resin are presented in Table 3.2.

Table 3.2 Material properties of 1K/T300 fibre and HexPly 913 epoxy resin (Mallikarachchi, 2019)

Material property	**T300 fibre**	**HexPly 913 epoxy resin**
Longitudinal Stiffness, E_1 (N/mm^2)	233000	3390
Transverse Stiffness, E_2 (N/mm^2)	23100	3390
Shear Stiffness, G_{12} (N/mm^2)	8963	1210
Poisson's Ratio, ν_{12}	0.2	0.41
Density, ρ (kg/m^3)	1760	1230
Areal weight of fabric/film, W (g/m^2)	98	30

Heterogeneous nature of the tow was idealised as a homogenised section with transversely isotropic properties as per the previous research studies. Even though the fibres and resin are two different materials, the overall material properties of tows should be calculated as a combination of both properties. The five independent engineering constants were calculated using the following methods and equations with the fibre volume fraction of the tow. The actual fibre volume fraction obtained from the micrograph is 0.62 (Mallikarachchi, 2019). Hence, the dry fibre model will have the same fibre volume fraction. However, in the resin embedded model, the additional resin added around the tows, will eventually increase the fibre volume fraction of the tows since, the overall fibre volume fraction should be maintained to the value of 0.62. In addition to that, the inclusion of voids in the resin geometry was also taken into account while calculating the new fibre volume fraction. Hence, the new fibre volume fraction of the tow is calculated as 0.88.

'Rules of mixtures' (Jones, 1998) was used to calculate the longitudinal extensional modulus and Poisson's ratio. Using Equations *(3. 1)* and *(3. 2)*,

$$E_1 = E_{1f}V_f + E_m(1 - V_f) \qquad (3.\ 1)$$

$$\nu_{12} = \nu_{13} = \nu_{12f} V_f + \nu_m (1 - V_f) \quad (3.\ 2)$$

Halpin-Tsai semi-empirical relation is used to evaluate the transverse extensional modulus as shown in the Equations

$$E_2 = E_3 = \frac{E_m(1+\chi\eta V_f)}{1-\eta V_f} \quad (3.\ 3)$$

$$\eta = \frac{E_{2f}-E_m}{E_{2f}+\chi E_m} \quad (3.\ 4)$$

Reinforcement of the composite depends on fibre geometry, packing geometry, and loading conditions. Here, the parameter χ was used to measure that the same. This parameter is taken as 2.0 for the calculation of transverse extensional modulus (Daniel, and Ishai, 2006).

Halpin-Tsai semi-empirical relation was used to estimate the shear modulus as well by considering χ as 1.0 (Daniel, and Ishai, 2006) and the empirical equation becomes as in Equation *(3. 5)*.

$$G_{12} = G_{13} = \frac{G_m\left((G_{12f}+G_m)+V_f(G_{12f}-G_m)\right)}{(G_{12f}+G_m)-V_f(G_{12f}-G_m)} \quad (3.\ 5)$$

In-plane shear modulus, G_{23} was estimated as Quek, Waas, Shahwan, and Agaram, 2003 mentioned in their study.

And, the transverse Poisson's ratio, ν_{23} was obtained by Equation *(3. 6)*,

$$G_{23} = \frac{E_2}{2(1+\nu_{23})} \quad (3.\ 6)$$

Table 3.3 shows the tow properties obtained using the above equations with fibre volume fractions of 0.62 and 0.88.

Table 3.3 Tow properties for fibre volume fractions 0.62, and 0.88

Material property	**Fibre volume fraction 0.62**	**Fibre volume fraction 0.88**
Longitudinal Stiffness, E_1 (N/mm^2)	145748.2	205446.8
Transverse Stiffness, $E_2 = E_3$ (N/mm^2)	10427.4	17462.1
Shear Stiffness, $G_{12} = G_{13}$ (N/mm^2)	3377.8	6138.1
Shear Stiffness, G_{23} (N/mm^2)	3498.0	6197.4
Poisson's Ratio, $\nu_{12} = \nu_{13}$	0.28	0.225
Poisson's Ratio, ν_{23}	0.49	0.409

Finally, the calculated material properties were fed and assigned into the dry fibre RUC models and the resin embedded RUC model in Abaqus finite element software respectively.

3.3.Development of the RUC Numerical Model for Multiscale Simulations

Dry fibre models have already been meshed in TexGen software using a series of python commands (refer Appendix A: Python code used in TexGen textile modelling software) and the tows were modelled using six-node linear triangular prism elements (C3D6) and eight-node linear reduced integration brick elements (C3D8R). This decision facilitates non-prismatic shapes and reduces any irrational increase in geometric stiffness.

However, for resin embedded models, meshes got vanished while exporting to Fusion 360 software. Hence, tows and resin are meshed by using the mesh function in Abaqus. Due to the non-linear edges and surfaces of the resin instance, ten-node quadratic tetrahedron elements (C3D10) were used to generate that resin part and similar to the dry fibre model, the tows were created using eight-node linear reduced integration brick elements (C3D8R).

3.3.1. Formulate Reference Points and Assign Multi Point Constraints

The RUC boundary acts as the connecting bridge to the neighbouring RUC. Therefore, every action such as applying load or enforcing boundary conditions must somehow involve the boundary nodes. Therefore, in some early research, Multi Point Constraints

(MPC) were used to connect all of boundary nodes each tow to a single reference point that was positioned in the mid of each tow (see Figure 3.7 All the boundary nodes of a tow are connected to one reference node). However, the issue is that it imposes rigid plate behaviour at the boundaries. It prevents any changes in cross section so that the entire cross section functions exactly like the respective reference node.

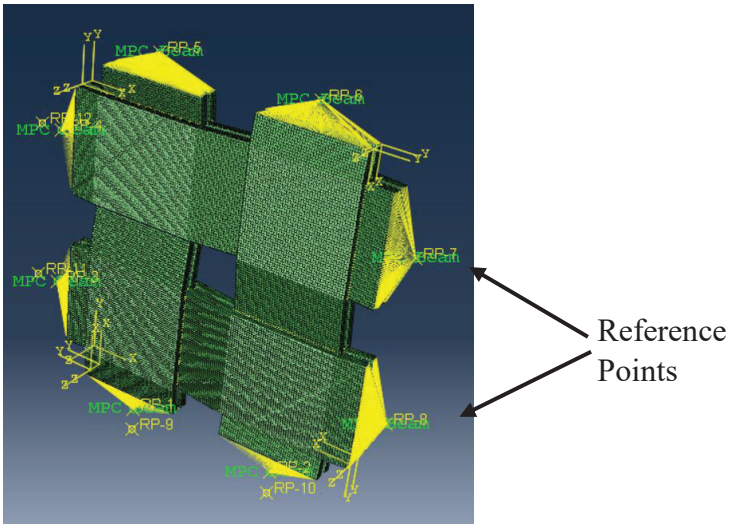

Figure 3.7 All the boundary nodes of a tow are connected to one reference node

Therefore, a small set of boundary nodes is connected to a distinct reference point assigned for each of them at the true neutral plane (refer Section 3.3.4.1) of RUC using multipoint constraints in order to avoid the rigid plate behaviour (see Figure 3.8).

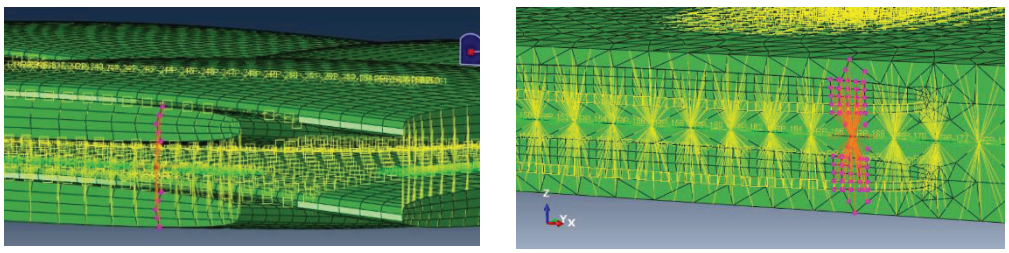

(a) Dry fibre model (b) Resin embedded model

Figure 3.8 Small set of boundary nodes connected to a distinct reference node

3.3.2. Enforcement of Periodic Boundary Conditions (PBC)

The main focus must be on the RUC to make sure that it accurately represents the woven laminate in its macroscale. The continuum nature of woven fibre laminate must

therefore be emphasized in RUC. Imposing PBC idealises the behaviour of the RUC based on the homogenized Kirchhoff-Love plate theory. The Abaqus/Standard FE program uses *EQUATION constraints to enforce these PBCs. The *EQUATION constraints of Abaqus/Standard require for two degrees of freedom and one prescribed nodal displacement or rotation in order to connect the two degrees of freedom linearly to one another. Such that, MPC control points (reference points) located at the opposite boundaries of RUC and a set of dummy nodes located at the two adjacent edges of RUC were connected using *EQUATION constraints (see Figure 3.9). Here, the first two inputs are the respective nodal degrees of freedom. The prescribed deformations were applied on the respective dummy node.

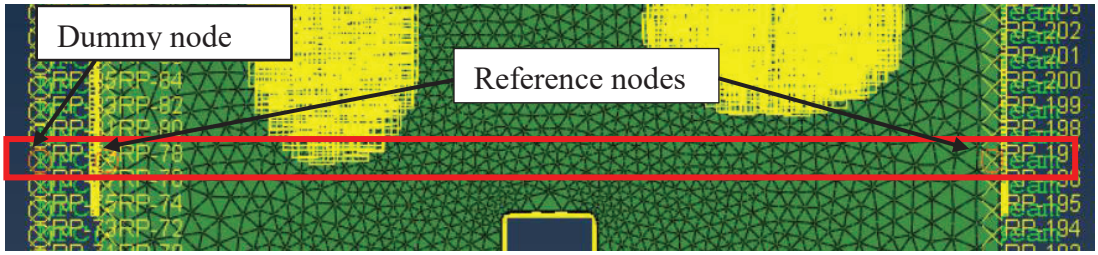

Figure 3.9 *EQUATION constraints application on resin embedded model

Similar to that, by using linear equations, all 6 degrees of freedom of the reference points which are located at both xz, and yz true neutral planes (refer Section 3.3.4.1), were constrained. The enforced constraint equations are shown in Equation *(3.7 A)* to Equation *(3. 7 K)*. Here, x, y, and z denote the coordinates of the node pair of X, Y, and Z axes respectively and the corresponding translations and rotations are denoted by u, v, w, and θ respectively. Direction of the deformation is denoted by the subscripts and the direction of a pair of boundary nodes is denoted by the superscripts. The PBCs take the forms;

$$\Delta u^x = \varepsilon_x \Delta L \qquad (3.7\ A)$$

$$\Delta v^x = \frac{1}{2}\gamma_{xy}\Delta L \qquad (3.7\ B)$$

$$\Delta w^x = -\frac{1}{2}\kappa_{xy} y \Delta L \qquad (3.7\ C)$$

$$\Delta {\theta_x}^x = -\frac{1}{2}\kappa_{xy}\Delta L \qquad (3.7\ D)$$

$$\Delta\theta_y{}^x = \kappa_x \Delta L \quad (3.7\ E)$$

$$\Delta\theta_z{}^x = 0 \quad (3.7\ F)$$

$$\Delta u^y = \frac{1}{2}\gamma_{xy}\Delta L \quad (3.7\ G)$$

$$\Delta v^y = \varepsilon_y \Delta L \quad (3.7\ H)$$

$$\Delta w^y = -\frac{1}{2}\kappa_{xy} x \Delta L \quad (3.7\ C)$$

$$\Delta\theta_x{}^y = -\kappa_y \Delta L \quad (3.7\ J)$$

$$\Delta\theta_z{}^y = 0 \quad (3.7\ K)$$

A Python programme was created to apply the periodic boundary conditions and multi-point constraints automatically for the RUC due to the repetitive nature of constraint enforcement (refer Appendix B: Python code used in ABAQUS FEM software to formulate reference nodes, dummy nodes, and constraints for the resin embedded model).

3.3.3. Apply Surface Based Cohesive Interactions

As described in Section 2.3.2, various methods have been used in earlier research studies to depict the interconnection between tows. However, the majority of the research used stiff connections like tie constraints and MPCs, where the link is between a node and a node or a node and a surface. The relative movement between tows was forbidden. Hence, Jayasekara (2019) considered the slipping behaviour between tows and used cohesive interaction between tow surfaces to increase the accuracy of the results in dry fibre models. Therefore, a surface based cohesive interactions are incorporated in this research study where the connection is only between two surfaces to eliminate the large penetration of slave nodes into the master surface.

The relevant traction stiffness coefficients of HexPly 913 epoxy resin have then been obtained from Jayasekara (2019). It was discovered by carrying out separate numerical analyses for resin under various fracture modes in accordance with Wijesuriya's technique (2019). The traction stiffness values for various failure modes are shown in Table 3.4

Table 3.4 Traction stiffness coefficients of HexPly 913 epoxy resin

Failure mode	Traction stiffness
Normal mode, K_{nn} (N/mm^2)	253 722
Shearing mode, K_{ss} (N/mm^2)	90 561
Tearing mode, K_{tt} (N/mm^2)	90 561

Surface based cohesive interactions were applied between two-two interface and tow-resin interface on both dry fibre RUC models and resin embedded RUC models respectively. First, the stiffness values were inserted into a newly created interaction property and then, the appropriate surfaces were selected manually and then interactions were created one by one (see Figure 3.10).

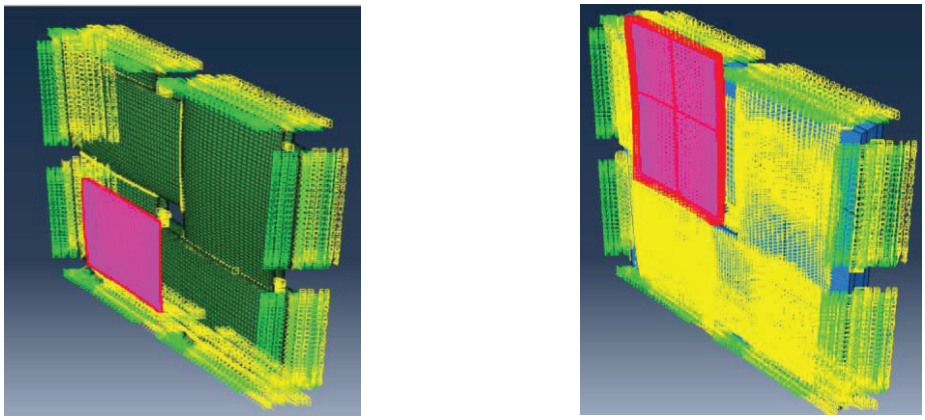

(a) Tow-tow interaction (b) Resin-tow interaction

Figure 3.10 Surface based cohesive interaction applied surfaces

3.3.4. Formulation of Boundary Value Problem

Predicting the macroscale mechanical behaviour is possible only if we design the microscale boundary value problems (BVPs) accurately. Starting from geometric modelling, obtain the accurate material properties, and enforcement of constraints have explained the crucial features of BVPs on the representative unit cell of woven fibre composite laminate. To complete the BVP definition, estimation of true neutral plane of the RUC with various phase shifts, application of unit deformations to obtain the mechanical properties, and usage of virtual work principle in extracting the macroscale mechanical properties are necessary.

3.3.4.1. Estimation of True Neutral Plane

Estimation of true neutral plane is crucial in order to avoid any anomalies in the results. Because, a research study on asymmetric weave single ply laminate (see Figure 3.11(a)) (Gao, et al., 2019) considered about the shift in neutral plane from mid plane and the consecutive effects on ABD stiffness matrix (see Figure 3.11(b)). This has not been considered in most of the studies. At the same time, relative positioning of tows may also cause asymmetric behaviour, eventually it may lead for inaccurate results. MPC control points and dummy nodes should lie on the true neutral plane of the RUC since they are the governing factors in the homogenised response of the woven composite. If the placement of those nodes is not in the true neutral plane, then there will be a residual bending moment during the axial load application.

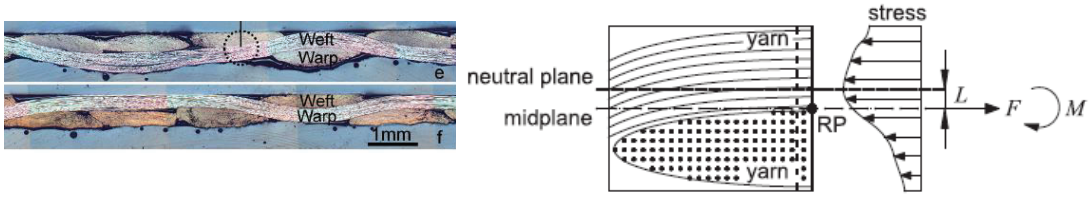

(a) (b)

Figure 3.11 (a) Cross-section of asymmetric weave, (b) Shift in neutral plane from the mid plane (Gao, et al., 2019)

Different true neutral planes were considered for xz and yz planes separately due to the unique tow distribution. An iterative method is carried out to find out the true neutral plane starting from an initial guess which is the apparent neutral plane of the RUC (geometric centre) rather than using the mid plane of the RUC as stated in Gao, et al., (2019). Apparent neutral plane estimations always very close to the true neutral plane because as per the theories, force resultant of a uniform stress field is transferred at the geometric centre of a given RUC boundary.

As shown in Figure 3.12, and Figure 3.13 the height of apparent neutral plane and true neutral plane on xz plane are denoted by $\hat{z}_x$ and $\bar{z}_x$ respectively and on yz plane are denoted by $\hat{z}_y$ and $\bar{z}_y$ respectively. As mentioned earlier, the initial guess for true neutral plane (apparent neutral plane) is considered as the geometric centre of the

specific RUC boundary. Geometric centre can be derived from the equations *(3.8 A)* and *(3. 8 B)* for x and y directions respectively.

$$\hat{z}_x = \frac{\sum_i A^i \hat{z}_x^i}{\sum_i A^i} \qquad (3.8\ A)$$

$$\hat{z}_y = \frac{\sum_i A^i \hat{z}_y^i}{\sum_i A^i} \qquad (3.\ 8\ B)$$

Here A was calculated using Table 3.1 And i denotes the tow identification number. Then, the correction on apparent neutral plane was done by an additive component to achieve the true neutral plane. This additive part is calculated by using an iterative method by considering force-moment relation *force = moment/normal distance* at the dummy nodes. Therefore, the true neutral plane of xz and yz plane are determined by the equations *(3.9 A)* and *(3. 9* B) respectively.

$$\bar{z}_x = \hat{z}_x + \sum_i (z_x^*)_i \qquad (3.9\ A)$$

$$\bar{z}_y = \hat{z}_y + \sum_i (z_y^*)_i \qquad (3.\ 9\ B)$$

Here $z_x^*, and\ z_y^*$ denote the additive correction factor calculated as the ratio between the bending moment and the axial force at a reference point on xz, and yz planes respectively. At the same time, z_x^* values from each i trial were summed up to avoid numerical errors. Trials were carried out until violating the condition, $\left(\frac{z_x^*}{\hat{z}_x}\right) < 0.01\%$. Similarly, $\bar{z}_y$ is calculated.

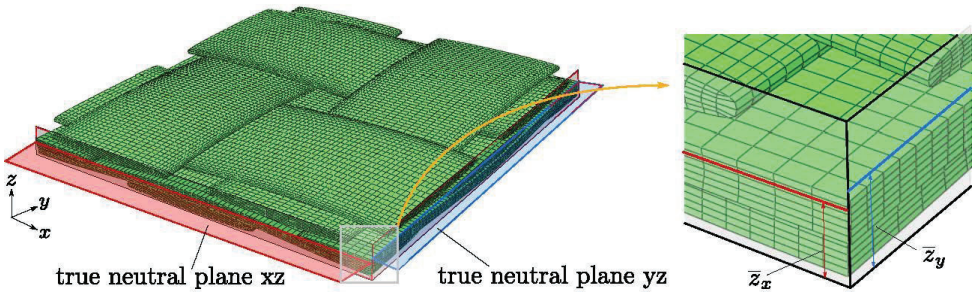

Figure 3.12 True neutral planes in both xz and yz planes for a RUC with 90° phase difference (Nishangani, et al., 2022)

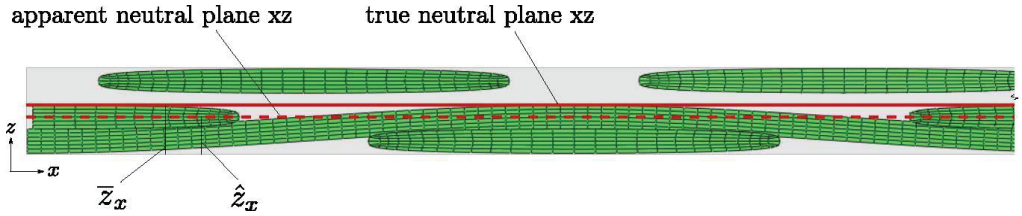

Figure 3.13 True and apparent neutral planes in xz plane for a RUC with 90° phase difference (Nishangani, et al., 2022)

3.3.4.2. Principle of Virtual Work for ABD Stiffness Matrix

Each entry of ABD stiffness matrix of woven fibre composite laminate is obtained using the virtual work principle. A combination of displacements and rotations were applied to the dummy nodes at the true neutral pane. Hence, by equating the external work done by the reaction forces/moments at the dummy nodes with the internal work done by the boundary nodes, the entries were found. Equation *(3. 10)* depicts that relationship for unit deformation in x direction,

$$N_{xx}\varepsilon_{xx}\Delta l_x\Delta l_y = \sum_{DN}(F_x u + F_y v + F_z w + M_x\theta_x + M_y\theta_y + M_z\theta_z) \qquad (3.\ 10)$$

Here, $\varepsilon_{xx} = 1$, and Δl_x and Δl_y denote the RUC lengths in x and y directions respectively. F and M are the forces and moments at the dummy nodes (DN). u, v, w are the displacements of the boundary reference points and θ are the rotations seen at the boundary reference points. Then, this summation was extended to all the dummy nodes. The first entry of the ABD stiffness matrix A_{11} can be obtained through the Equation *(3. 11)*, by substituting $\varepsilon_{xx} = 1$,

$$A_{11} = \frac{\sum_{DN}(F_x u + F_y v + F_z w + M_x\theta_x + M_y\theta_y + M_z\theta_z)}{\Delta l_x \Delta l_y} \qquad (3.\ 11)$$

This clearly illustrates how the microscale local forces and displacements are mapped with the macroscale homogenised sections. Here, if unit deformation in x direction is considered, then the other strains and rotations will be set to zero ($\varepsilon_y = \gamma_{xy} = \kappa_x = \kappa_y = \kappa_{xy} = 0$). Similar to that, considering each unit deformation at a time, 6 separate analyses were carried out in order to obtain the whole ABD matrix.

A pre-developed and modified MATLAB code (see Appendix C: MATLAB code used to calculate the ABD matrix of Resin embedded model) was used to calculate the ABD stiffness matrix using the extracted force resultants and displacements from dummy nodes and reference points respectively.

4. ANALYSIS OF RESULTS

Three different dry fibre RUC models with varying phase shifts (30°, 45°, 60°) were analysed in the linear regime to capture the variation in mechanical properties due to the relative positionings. Then the ABD matrices 0°, 90°, and 180° phase difference models were extracted from Nishangani (2021) for covering the complete range from 0° to 180°. Then, a resin embedded in-phase RUC model was analysed in the non-linear regime to obtain the moment curvature relationship. The numerical results obtained are validated with experimental results available in literature.

4.1. Results of Dry Fibre RUC Models with Varying Phase Differences

4.1.1. ABD matrices

ABD stiffness matrices obtained from each analysis are shown in the Equations *(4. 1)* to *(4. 3)*, These were obtained following the approach discussed in detail under Section 3.3.4. Herein, the notation ABD_θ is used, where θ refers to the considered phase difference.

$$ABD_{30^\circ} = \begin{pmatrix} 10260 & 1186 & -14 & 0.2 & -1 & -2 \\ 1186 & 10209 & -8 & -9 & 4 & -4 \\ -14 & -8 & 396 & -0.7 & -0.6 & -0.2 \\ 0.2 & -9 & -0.7 & 36 & 1 & -0.2 \\ -1 & 3 & -0.6 & 1 & 35 & -0.2 \\ -2 & -3 & -0.2 & -0.2 & -0.2 & 3 \end{pmatrix} \quad (4.\ 1)$$

$$ABD_{45^\circ} = \begin{pmatrix} 10304 & 1106 & -1 & 0.9 & 4 & 0 \\ 1106 & 10286 & -4 & 1 & 3 & -0.2 \\ -1 & -4 & 279 & 0.2 & -0.1 & -0.8 \\ 0.9 & 1 & 0.2 & 35 & 2 & 0 \\ 4 & -3 & -0.1 & 2 & 35 & 0 \\ 0 & -0.2 & -0.9 & 0 & 0 & 3 \end{pmatrix} \quad (4.\ 2)$$

$$ABD_{60^\circ} = \begin{pmatrix} 10655 & 902 & -9 & -1 & 4 & 3 \\ 902 & 10646 & -0.7 & 1 & -2 & 7 \\ -9 & -0.7 & 425 & -0.5 & 0.5 & 3 \\ -1 & 1 & -0.5 & 35 & 3 & -0.4 \\ 4 & -2 & 0.5 & 3 & 35 & -0.2 \\ 3 & 7 & 3 & -0.4 & -0.2 & 4 \end{pmatrix} \quad (4.\ 3)$$

Anomalies, such as non-zero *B* sub-matrix and minor asymmetric entries in the ABD matrix, have been observed in all matrices and most of them are be negligible. However, some axial - coupling entries, axial – bending coupling entries, and bending-twisting coupling entries are considerable. These are expected to be an outcome of irregularities in selecting the contact surfaces between tows, and idealisation on fibre-resin interactions. ABD stiffness matrices obtained for 0°, 90°, and 180° phase difference RUC models are provided in Appendix D: ABD matrices of fibre in-phase, 90° phase shift, and fibre out-of-phase RUC models..

4.1.2. Comparison with Experimental Results and CLT Results

Classical lamination theory predictions are included here for the comparison with the finite element results, and experimental results. As mentioned in the section 2.3.1, CLT is efficient for unidirectional laminates. Hence, an approximate estimation of the elastic modulus was done according to the equation *(4. 5)* and using Table 3.2. Here, the coefficient of 0.5 is used in this equation due to the ½ of the fibres are in transverse direction (Soykasap, 2006).

$$E_1' = 0.5V_f E_{1f} + V_m E_m \qquad (4.\ 4)$$

Then, using the equations *(4. 5)* and, *(4. 6)* bending stiffness and axial stiffness values were calculated and tabulated in . Where, t – laminate thickness which is 0.236 mm.

$$D_{11\_CLT} = \frac{E_1' t^3}{12(1-\nu_{12}^2)} \qquad (4.\ 5)$$

$$A_{11\_CLT} = \frac{E_1' t}{1-\nu_{12}^2} \qquad (4.\ 6)$$

Table 4.1 Classical lamination theory predictions

E_1'	73518 N/mm^2
D_{11_CLT}	87.4 Nmm
A_{11_CLT}	18826 N/mm

The predictions of CLT is plotted with finite element results and experiment results in Figure 4.1 and Figure 4.2. As mentioned in section 2.3.1, it overpredicts the mean experimental results of bending and axial stiffnesses by 132%, 46% respectively.

Comparisons between experiment findings and FEM results of the extensional stiffness and shear stiffness will be accurate if the inverse of the A sub matrix of the corresponding ABD stiffness matrix is considered. Because the tension tests used narrow specimens in order to ensure that the transverse and shear stress resultants are negligible, such that $N_y \approx N_{xy} \approx 0$ at the mid part of the specimen (Mallikarachchi, 2011). Hence, a 3×3 compliance matrix can be defined as in the equation *(4. 7)*.

$$\begin{Bmatrix} \varepsilon_x \\ \varepsilon_y \\ \gamma_{xy} \end{Bmatrix} = \begin{bmatrix} a_{11} & a_{12} & a_{16} \\ a_{12} & a_{22} & a_{26} \\ a_{16} & a_{26} & a_{66} \end{bmatrix} \begin{Bmatrix} N_x \\ N_y \\ N_{xy} \end{Bmatrix} \qquad (4.\ 7)$$

Substituting $N_y = N_{xy} = 0$ on the equation *(4. 7)* results in equation *(4. 8)*,

$$\varepsilon_x = a_{11} N_x \qquad (4.\ 8)$$

After finding the inverse of the appropriate entries in compliance matrix and respective experiment results can be compared since the experiments measure the deformations caused by unit loads. Hence, the axial stiffness can be obtained by equation *(4. 9)*

$$\text{Axial stiffness} = \frac{N_x}{\varepsilon_x} = \frac{1}{a_{11}} \qquad (4.\ 9)$$

On the other hand, the bending stiffness was measured using four-point bending tests conducted on wider specimens. Therefore, the transverse and twisting curvatures were negligible, ($\kappa_y \approx \kappa_{xy} \approx 0$). Hence, measured bending stiffness can be directly compared with D_{11} of the ABD matrix. Substituting $\kappa_y = \kappa_{xy} = 0$ in equation *(4. 10)* results(4. 11),

$$\begin{Bmatrix} M_x \\ M_y \\ M_{xy} \end{Bmatrix} = \begin{bmatrix} D_{11} & D_{12} & D_{16} \\ D_{12} & D_{22} & D_{26} \\ D_{16} & D_{26} & D_{66} \end{bmatrix} \begin{Bmatrix} \kappa_x \\ 0 \\ 0 \end{Bmatrix} \qquad (4.\ 10)$$

$$M_x = D_{11} \kappa_x \qquad (4.\ 11)$$

$$\text{Bending stiffness} = \frac{M_x}{\kappa_x} = D_{11} \quad (4.\ 12)$$

Poisson's ratio can be found as,

$$\nu_{12} = -\frac{a_{21}}{a_{11}} \quad (4.\ 13)$$

Finally, the variations of the axial stiffness, shear stiffness, bending stiffness, twisting stiffness values, and Poisson's ratio were obtained accordingly over the phase differences and were plotted along with the experimental results obtained from Mallikarachchi, (2011). Here, in accordance with the micrograph shown in Figure 1.8 Micrograph of two-ply plain weave laminate , it is clear that the phase angle varies along the weave length. Additionally, there is no guarantee that the specimens used were having the same phase angle. Hence, the experimental results were plotted as mean values with appropriate standard deviations.

The variation of in-plane properties of thin woven fibre composite obtained from finite element modelling are plotted over the tow phase differences shown in Figure 4.1. Axial stiffness in both x and y directions ($1/a_{11}$ and $1/a_{22}$) shows a similar variation along the phase difference as expected due to the orthotropic nature. They depict an increase of 27% while shifting the top ply by 30° from fibre in-phase configuration. Then they reach a maximum of about 10568 N/mm at 60° and then reduces until 180° at a low rate and attain a value around 9371 N/mm. However, in comparison with experiment results, the finite element results are under-predicted. Shear stiffness does not show a considerable fluctuation along with the phase difference i.e: it almost a flat line as in the Figure 4.1 Variation of in-plane properties over tow phase difference thus, the effect of relative positioning of tow on the shear stiffness in negligible.

Figure 4.2 depicts the variation of the experiment results obtained under four-point bending test for six specimen and the out-of-plane properties of thin woven fibre composite obtained through FEM over the phase angle difference. Similar to extensional stiffnesses, bending stiffnesses in both x and y directions (D_{11} and D_{22}) shows almost the same behaviour. There is a 4% reduction observed in the bending stiffness while moving from 0° to 45° and it reaches the minimum at 45°. No

noticeable changes are there between 45° to 90°. A slight increase of 9% has been noted between 90° to 180° and it attains its maximum of 38.6 Nmm/mm at 180°. Interestingly, the whole finite element results fall within the acceptable tolerance limit of the experiment results obtained by Mallikarachchi, (2019). This acceptable fluctuation in the bending stiffness values are the result of the true neutral plane consideration which reduces the leaver arm between the axial resultant forces. Considerable variation on twisting stiffness has been identified between 0° to 90° and it reaches the maximum of 3.9 Nmm/mm at 60° and then drops by 56% at 90°.

Considerable change in the Poisson's ratio has been observed over the phase difference of the tows (see Figure 4.3). A steep drop of 52% is observed in the Poisson's ratio while moving from 0° to 30°. Then it continues to decrease up to 0.08 and touches that minimum at 60°. Starting from 30° to 180°, the Poisson's ratio predictions fall within the acceptable tolerance limits of the experiment results (Mallikarachchi, 2019).

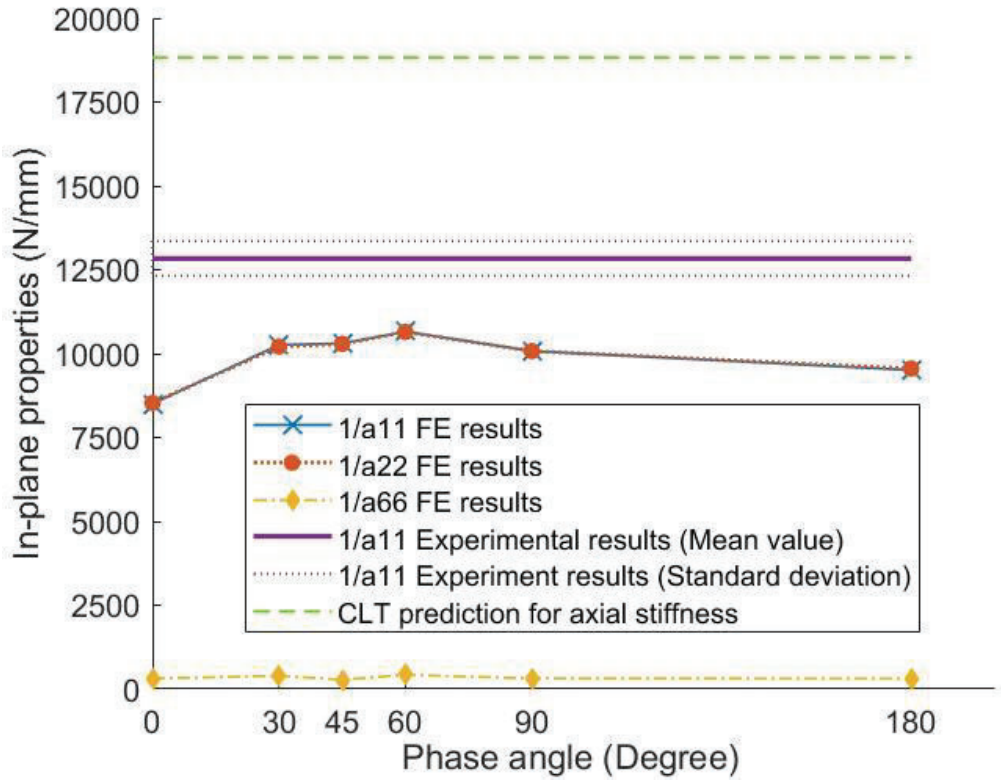

Figure 4.1 Variation of in-plane properties over tow phase difference

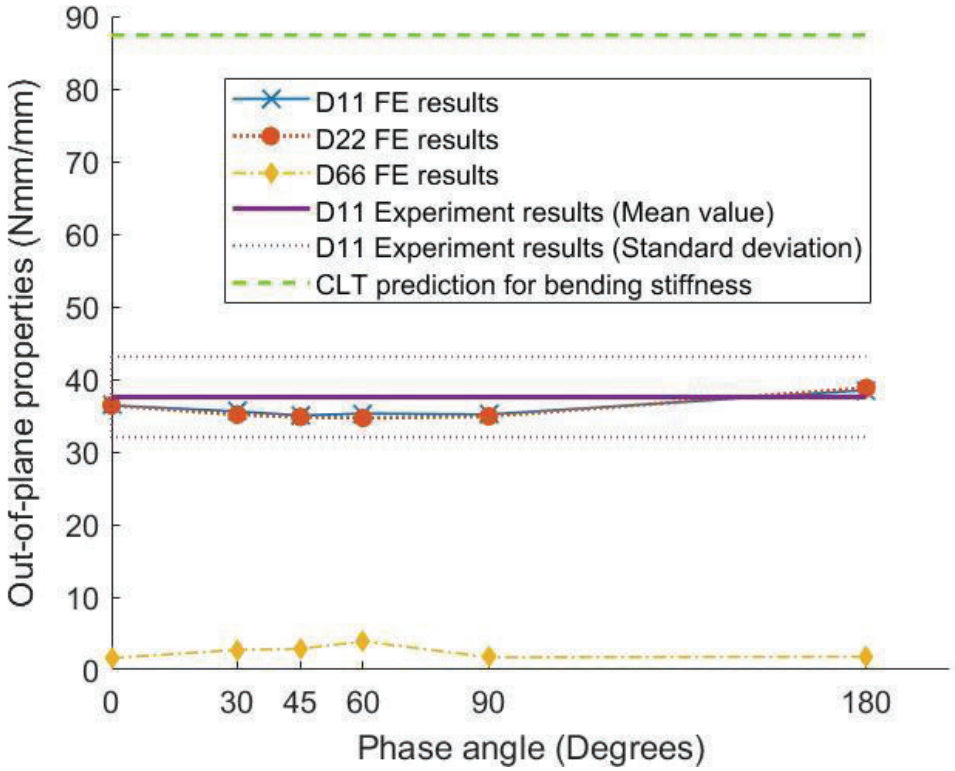

Figure 4.2 Variation of out-of-plane properties over tow phase difference

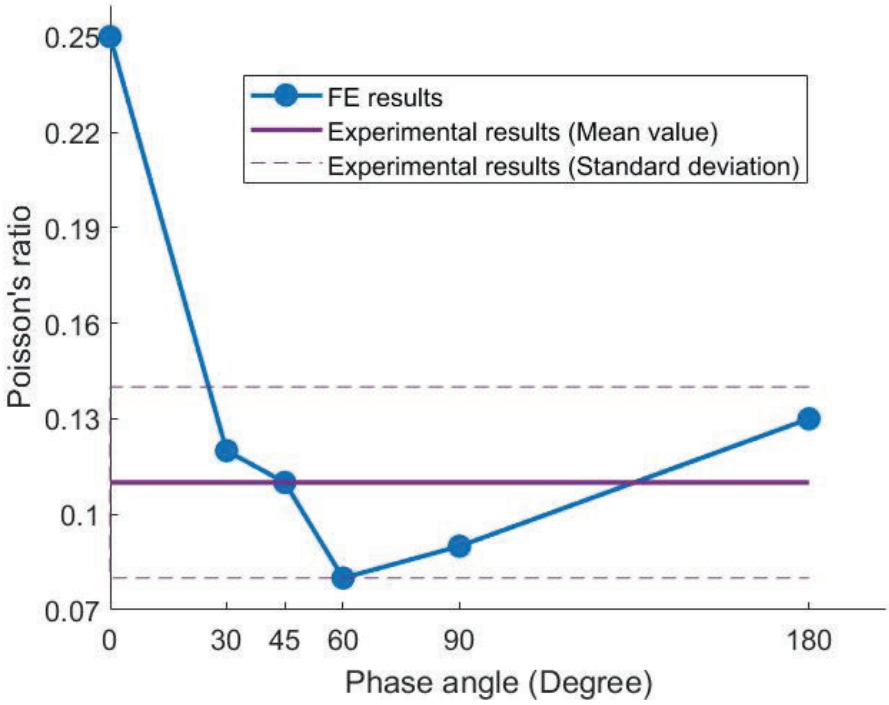

Figure 4.3 Variation of Poisson's ratio over tow phase difference

4.2. Results of Resin Embedded RUC Model

4.2.1. Linear Analysis Results

ABD stiffness matrix obtained from the linear analysis of the resin embedded RUC model shown in the equation *(4. 14)*

$$ABD_{resin\ emb.} = \begin{pmatrix} 12682 & 1553 & 1 & 141 & 1 & 0 \\ 1563 & 14139 & -1 & 22 & 1 & 0 \\ 2 & -1 & 1384 & 1 & -1 & 1 \\ 142 & 22 & 0 & 52 & -2 & 0 \\ 1 & 1 & 0 & 2 & 60 & 0 \\ 21 & 39 & -10 & 0 & 0 & 6 \end{pmatrix} \quad (4.\ 14)$$

Anomalies have been observed in most of the sub-matrices and some are negligible. However, there is a considerable coupling between axial and bending stiffness which cannot be ignored. In addition to that, A_{11}, and D_{11}should be equal to A_{22}, and D_{22} respectively since tows in both x and y directions are having the same properties. *(2. 7)*The deviations observed are around 11% and 15% respectively. This might be due to the dissimilarities in selecting the contact surfaces for the application of cohesive interaction between two tow surfaces and between resin and tow surfaces. Hence, the resin embedded RUC model has to be modified further in order to eliminate these anomalies.

The appropriate stiffness values were calculated as explained in section 4.1.2 and tabulated in Table 4.2 with the experimental outcomes (Mallikarachchi, 2019).

Table 4.2 Comparison of the results from the analysis of resin embedded RUC model with experimental results

Description	$\frac{1}{a_{11}}$ (N/mm)	$\frac{1}{a_{66}}$ (N/mm)	D_{11} (Nmm/mm)	v_{12}
Experiment Results	12833 ± 517	833.3	37.55 ± 5.54	0.11 ± 0.03
Resin embedded model	12510	1383.6	52.11	0.11
Percentage deviation	2.5%	66%	38.7%	0%

This resin embedded RUC model predicted the axial stiffness and Poisson's ratio with good accuracy as the deviation percentage itself falls within the accepted tolerance limit from the experiments. However, it overpredicts the shear stiffness by 66%

because, the shear response mainly depends on the behaviour of the interactions applied. Here, due to the additional resin around the tows, the number of interaction surfaces have increased compared to dry fibre models where the dry fibre models underpredicted the shear stiffness by 62% (Nishangani, 2021). Hence, to improve the shear stiffness predictions, further concerns should be given on applying more suitable interaction types and properties.

Similarly, the bending stiffness value is also overpredicted by 38.7% in comparison with the experiment results. The reason could be the possible existence of voids in the resin. Even though the void located at the mid part of the RUC is considered in this study, there are possibilities for some more voids in the edges and corners of the RUC. In addition to that, the additional resin around the tows increases the fibre volume fraction of the tow in order to maintain the overall fibre volume fraction measured in the experiment (refer section 3.2) which plays a significant role in increasing the bending stiffness. Similar observation was made in various research studies done on resin embedded RUC models of two-ply plain weave laminate with different fibre volume fractions such as 0.68 (Mallikarachchi, 2011), 0.75, (Jayasekara, 2020), 0.74 (Weerasinghe, 2022). Hence, further improved predictions can be obtained by keeping the appropriate volume of the resin around the tows which resembles the actual experimental specimen having undulations on the surfaces.

4.2.2. Non-linear Bending Response

Considering the deformed non-linear geometry of the RUC, this analysis is carried out. Some minor changes in the input file is adequate to incorporate the effects of geometric nonlinearity in the analysis. Adding the NLGEOM parameter to the *STEP option initiates the non-linear analysis. An alternate method used in graphical user interface is, to turn on *nlgeom* in the 'step' module. It is possible to specify the maximum number of increments allowed during a step by adding INC parameter. However, limiting the maximum number of increments might terminate the analysis, if it is not adequate. Hence to avoid that, 20 steps were defined with an increasing curvature of 0.01 mm^{-1} at each step, starting from 0 to 0.2 mm^{-1}. The results obtained are plotted as moment-curvature relationship in Figure 4.4.

The developed resin embedded RUC model overpredicts the bending stiffness throughout the curvature range considered starting from 0 to 0.203 mm^{-1}. The obtained moment curvature response shows an increasing slope until 0.15 mm^{-1} and then starts to decrease till the curvature at failure (0.203 mm^{-1}). Hence, the resin embedded RUC model has to be modified further as suggested in the section 4.2.1 for improved and acceptable predictions.

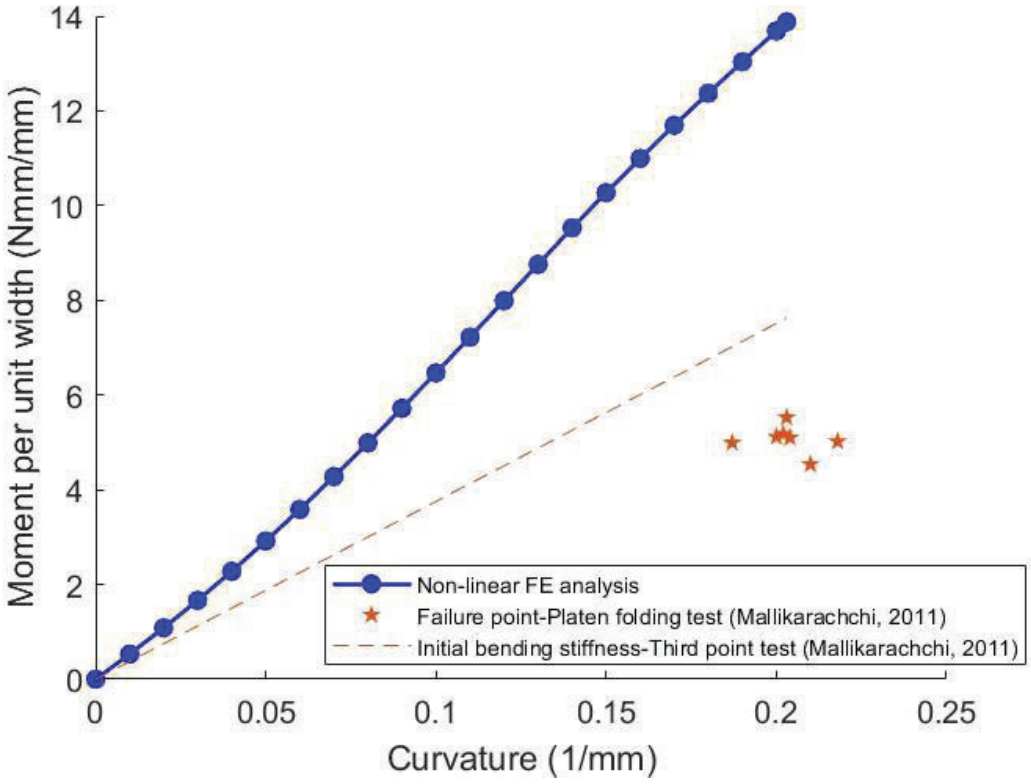

Figure 4.4 Moment-curvature response of resin embedded RUC in comparison with experiment results

5. CONCLUSION AND RECOMMENDATION

A research study on predicting the mechanical properties of ultra-thin woven fibre composite laminates has been presented in this dissertation. The mechanical properties have been obtained in detail through numerical models of representative unit cells of two-ply plain weave carbon fibre reinforced polymer laminates. The basic steps involved are, incorporating the necessary geometric properties, material properties and appropriate boundary conditions into the numerical models of the RUCs and then the required stiffness values were extracted using a pre-developed and modified python code.

The main objectives of this research study were, (i) to study the effect of varying fibre orientation (relative positioning of fibres with respect to each other) on mechanical properties, (ii) to predict nonlinear bending properties under high curvatures considering the effects of variation in fibre-matrix interactions. The major accomplishments and problems are summarised here and future research directions are presented.

5.1. Important Findings and Discussion

First, a parametric study on the homogenised response of carbon fibre thin woven composites is performed to address the fluctuations in the ABD stiffness matrix entries for a series of relative positionings of tows. Starting from 0°, 30°, 45°, 60°, 90°, and 180° phase angles were considered in this research. The outcomes of this study show an intriguing variations in the entries of ABD stiffness matrix along with different phase angles. A significant variation is observed in the in-plane properties except for the shear stiffness and minor changes are seen on out-of-plane properties along with the phase angles. This observation proves that a significant importance should be given on the inter-ply misalignment during the manufacture of these composites. Hence, it concludes that assuming fibre in-phase configuration (0°) for the unit cell that actually with a varying phase shifts along the weave length will provide non-reliable outcomes. Even though, a significant variation in extensional stiffness with respect to phase difference is obtained, those values are still underpredicted compared to the experimental results. This issue might be solved by introducing appropriate

volume of resin in between the tows which will increase the fibre volume fraction within the tows to maintain the overall fibre volume fraction of the unit cell. According to this observation, it is clear that, the first objective of this research study is achieved since variation on mechanical properties have been captured well along with varying phase differences.

Next, the analysis on the resin embedded RUC model concludes that, the prediction of axial stiffness and Poisson's ratio obtained through numerical linear analysis, validates the experiment results with good accuracy where, the deviations observed between the experimental results are 2.5% and 0% respectively. However, the shear stiffness values are over predicted by a considerable margin. This is because of the increased number of interactions introduced due to the additional resin around the tows. Hence, this may be reduced significantly by decreasing the thickness of the resin part around the tows which eventually reduces the contact surface area for the interactions. Similarly, higher bending stiffness predictions in both linear and non-linear analysis are observed compared to the experimental results. This could be due to existence of additional voids in the resin and/ or due to the ignorance of resin damage initiation and propagation on composites under high curvatures, and intra-ply damage. With regards to this analysis results, the moment curvature response has been derived but, this resin embedded unit cell model has not been able to capture the reduction in bending stiffness as expected. Hence, the second objective of this research is not fully achieved due to the limitations in time and resources and further developments (refer Section 5.2) on the unit cell model is crucial for improved predictions.

5.2. Recommended Future Works

Future works required on dry fibre unit cell model and resin embedded unit cell model to improve the accuracy of the results and to the eliminated the abnormal behaviours observed in the obtained results are listed below.

Dry fibre unit cell model

- ❖ Inclusion of appropriate volume of additional resin in the dry fibre RUC model may improve the predictions of in-plane properties

- ❖ In accordance with the manufacturing process, the phase shift may occur in only one direction. Hence, relative positioning in either x or y direction should be studied further

Resin embedded unit cell model

- ❖ Understanding the manufacturing process of the woven fibre composite laminate is crucial to address the minor details that may affect the results by a considerable margin. Hence, by considering two different procedures, the geometry of the unit cell can be developed in two different ways. Those are,
  - reducing the thickness of the resin around the unit cell from both top and bottom faces of the RUC
  - reducing the resin thickness from either top or bottom face of the RUC

- ❖ Additional and possible voids in the woven fibre composite need to be addressed carefully for improved accuracy of the results

6. REFERENCE LIST

Bednarycyk, B. A. & Arnold, S. M., 2003. Micromechanics-Based Modeling of Woven Polymer Matrix Composites. *AIAA Journal,* 41(9), pp. 1788-1796.

Bilisik, K., 2012. Multiaxis three-dimensional weaving for composites: A review. *Textile Research Journal.*

Chahat, N. et al., 2017. Deep Space Network Telecommunication CubeSat Antenna: Using the deployable Ka-band mesh reflector antenna. *IEEE Antennas and Propagation Magazine,* pp. 1-1.

Cox, B. N., Carter, W. C. & Fleck, N. A., 1994. A binary model of textile composites-I: formulation.

Ferreira, A. D. B. L, Novoa, P. R. O, and Marques, A. T, 2016. Multifunctional MAterial Systems: A state-of-the-art review. *Composite Structures 151,* pp. 3-35.

Foust, J., n.d. *Space news.com.* [Online] Available at: https://spacenews.com/nasa-investigating-issue-with-lucy-solar-array/ [Accessed 10 June 2022].

Gao, J. et al., 2019. A multi-scale method for predicting ABD stiffness matrix of single-ply weave-reinforced composite. *Composite Structures,* September.230(111478).

Gibson, R. F., 2016. *Principles of Composite.* 4 ed. s.l.:s.n.

Grumman, N., n.d. *Northropgrumman.com.* [Online] Available at: https://www.northropgrumman.com/space-old/astro-aerospace-products-telescopic-tube-masts/

Hamillage, M. Y., Kwok, K. & Fernandez, J. M., 2019. *Micromechanical Modelling of High-Strain Thin-Ply Composites.* s.l., s.n.

Hamillage, M. Y. & Mallikarachchi, H. M. Y. C., 2017. *Predicting non-linear bending behaviour of thin woven fibre composites.* s.l., s.n.

Herath, S. & Mallikarachchi, C., 2016. Modified Ply Thickness for Classical Lamination Theory for Thin Woven Fibre Composites.

Ichihashi, H., Hamada, H., lkuta, N. & Maekawa, Z., 1994. *Finite element analysis of woven fabric composites considering interfacial properties.* Japan, s.n.

Jayasekara, M., 2020. *Non-linear Bending Behaviour of Thin Woven Fibre Composites Under High Curvatures,* s.l.: University of Moratuwa.

Johnson, Todd, 2018. *History of Composites.* s.l.:s.n.

Jones, R. M., 1998. *Mechanics of composite materials.* 2 ed. Philadelphia: PA:CRC Press.

Karkkainen, R. L. & Sankar, B. V., 2006. A direct micromechanics method for analysis of failure initiation of plain weave textile composites. *Composites Science and Technology,* 66(1), pp. 137-150.

Kueh, A. & Pellegrino, S., 2007. *ABD Matrix of Single-Ply Triaxial Weave Fabric.* s.l., s.n.

Kwok, K. & Pellegrino, S., 2016. Micromechanics Models for Viscoelastic Plain-Weave Composite Tape Springs. *AIAA Journal,* October, 55(1), pp. 309-321.

Mallikarachchi, C. & Pellegrino, S., 2011. *Design and validation of thin-walled composite deployable booms with tape-spring hinges.* s.l., s.n.

Mallikarachchi, H. M. Y. C., 2011. *Thin-Walled Composite Deployable Booms with Tape-Spring Hinges,* s.l.: s.n.

Mallikarachchi, H. M. Y. C., 2019. Predicting mechanical properties of thin woven carbon fiber reinforced laminates. *Thin-Walled Structures 135,* pp. 297-305.

Mallikarachchi, H. M. Y. C. & Pellegrino, S., 2008. *Simulation of quasi-static folding and deployment of ultra-thin composite structures.* s.l., s.n.

Mallikarachchi, H. M. Y. C. & Pellegrino, S., 2013. Failure criterion for two-ply plain weave CFRP laminates. *Journal of Composite Materials,* May, 47(11), pp. 1357-1375.

Mao, J. et al., 2013. A Modeling Approach Across Length Scales for Progressive Failure Analysis of Woven Composites. *Applied Composite Materials,* June, Volume 20, pp. 213-231.

Múgica, J. I. et al., 2019. Multiscale modelling of thermoplastic woven fabric composites: From micromechanics to meso mechanics. *Composite Structures,* 20 August.

Nadarajah, S., Jayasekara, M. & Mallikarachchi, C., 2019. *Nonlinear Bending Response of Two-Ply Plain Woven Carbon Fibre Composites.* s.l., s.n., pp. 147-151.

Nishangani, G., 2021. *Influence of relative positioning of tows on mechanical properties of thin woven composites,* s.l.: s.n.

Nishangani, G., Jayasekara, M., Mallikarachchi, C. & Herath, S., 2022. Effcets of tow arrangements on homogenized response of carbon fiber woven composites. *Composite Structures,* 15 November.Volume 300.

Sakovsky, M., Pellegrino, S. & Mallikarachchi, H. M. Y. C., 2016. *Folding and Deployment of Closed Cross-Section Dual-Matrix Composite Booms.* San Diego, California, USA, s.n.

Sanford, G., Biskner, A. & Murphey, T., 2010. *Large Strain Behavior of Thin Unidirectional Composite Flexures.* s.l., s.n.

Soykasap, O., 2006. Micromechanical models for bending behavior of woven composites,. *Journal of Spacecraft and Rockets,,* 43(5), pp. 1093-1100.

Soykasap, O., Pellegrino, S., Howard, P. & Notter, M., 2008. Folding Large Antenna Tape Spring. *Journal of Spacecraft and Rockets,* 45(3), pp. 560-567.

Soykasap, O., Watt, A. M. & Pellegrino, S., 2004. *New Deployable Reflector Concept.* s.l., s.n.

Swetha Lakshmi, S. et al., 2022. *Thermo-structural analysis of deployable composite booms with slotted hinges for space applications.* s.l., s.n., pp. 3564-3570.

TexGen, 2018. *User Guide v3.10,* s.l.: University of Nottingham Textile Composites Research, Nottingham.

Thomson, S., 1999. *The AstroMesh Deployable Reflector.* s.l., s.n., pp. 1516-1519.

Twfik, B., Leheta, H., Elhewy, A. & Elsayed, T., 2016. Weight Reduction and strengthening of marine hatch covers by using composite materials. *International Journal of Naval Architecture and ocean Engineering 9(2).*

Ubamanyu, K. & Mallikarachchi, H. M. Y. C., 2016. *Simulation of dual-matrix composite boom.* s.l., s.n.

Weerasinghe, U., 2022. *Homogenization of Ultra Thin Woven Composite Structure at High curvatures,* s.l.: s.n.

Wijesuriya, H., Deemantha, C., Nadarajah, S. & Mallikarachchi, C., 2018. *Predicting bending behaviour of deployable booms made of thin woven fibre composites.* s.l., s.n.

Woo, K. & Suh, Y. W., 2001. Low degree of homogeneity due to phase shift for woven textile composites. *Comps Sci Technol,* 23(4).

Woo, K. & W., S. Y., 2001. Low degree of homogeneity due to phase shift for woven textile composites. *Compos Sci Technol,* 23(4).

Yee, J. C. H. & Pellegrino, S., 2005. Folding of Woven Composite Structures. *Composites/A,* 36(2), pp. 273-278.

7. APPENDICES

Appendix A: Python code used in TexGen textile modelling software

```
% Read the textile

    textile=GetTextile('Textile Name')

% Read the Yarn (Tow)

    yarn = textile.GetYarn(Tow Number);

% Setting the number of mesh layers in longitudinal direction

    yarn.SetResolution(Number of mesh layer needed);

% Set the cross section

    section=CSectionPowerEllipse(width, thickness, power);

% Setting the number of mesh layers through thickness

    section.SetSectionMeshLayers(number of mesh layer needed);

% Assign mesh

    yarn.AssignSection(CYarnSectionConstant(section));
```

Appendix B: Python code used in ABAQUS FEM software to formulate reference nodes, dummy nodes, and constraints for the resin embedded model

```
# -*- coding: mbcs -*-

from part import *
from material import *
from section import *
from assembly import *
from step import *
from interaction import *
from load import *
from mesh import *
from optimization import *
from job import *
from sketch import *
from visualization import *
from connectorBehavior import *
# * Number of intervals must be greater than zero.
#Model parameters
a = 2.664
b = 2.664
meshSize = 0.015
eps = meshSize/10 #0.0015 used 0.00075 in one tow
maxtowheight = 0.059
###### RUC mid point z value = 0 ######
towwidth = 1.013
towlength = a

Model = mdb.models['Model-1']

# mdb.models[name].parts[name]
Model.parts['Resin']
Model.parts['Tow_0']
Model.parts['Tow_1']
Model.parts['Tow_2']
Model.parts['Tow_3']
Model.parts['Tow_4']
Model.parts['Tow_5']
Model.parts['Tow_6']
Model.parts['Tow_7']

n1 = Model.rootAssembly.instances['Resin-1'].nodes
n2 = Model.rootAssembly.instances['Tow_0'].nodes
n3 = Model.rootAssembly.instances['Tow_1'].nodes
n4 = Model.rootAssembly.instances['Tow_2'].nodes
```

```
n5 = Model.rootAssembly.instances['Tow_3'].nodes
n6 = Model.rootAssembly.instances['Tow_4'].nodes
n7 = Model.rootAssembly.instances['Tow_5'].nodes
n8 = Model.rootAssembly.instances['Tow_6'].nodes
n9 = Model.rootAssembly.instances['Tow_7'].nodes

ra = Model.rootAssembly
nfile = open('MeshCoordinates.txt','w+')
#Create equation constraints
                    Pick nodes of face Z = 0.00 (face1)
              → Corresponding to the mid plane of RUC
;considering both top and bottom boundary nodes as one set
#n = ins.nodes
n = n1 + n2 + n2 + n4 + n5 + n6 + n7 + n8 + n9
face1 = n.getByBoundingBox(−1.0 ∗ (eps), −1.0 ∗ (eps), −1.0 ∗ (eps), a
              + eps, b + eps, 1.0 ∗ eps)
### 0.00 (−0.057 to − 0.061 mm variation on mid plane of the bottom ply)
#Create text file
eqFile = open('periodicBC.dat','w+')
eqFile1 = open('periodicBC.txt','w+')

P1count = 1
Q1count = 1
R1count = 1
S1count = 1

RefNodesPR = 1

RefPoint_X1 = list(range(37))## (18 + 1 + 18 = 37) Resin nodes
RefPoint_Y1 = list(range(37))
#RefPoint_X2 = list(range(80))
#RefPoint_Y2 = list(range(80))

#Iterate over the nodes of 2
              − ply RUC. face1 refers to midplane of the whole RUC
for II in range(len(face1)):
  #Coordinates of II − th node
  n_1 = face1[II]
  coords = n_1.coordinates
  x1 = coords[0]
  y1 = coords[1]
  z1 = coords[2]

  if z1 < 1 ∗ eps and z1 >= −1 ∗ eps: ##(0.00)
    if y1 <= 0.0 + 0.1 ∗ eps or y1 >= b − 0.1 ∗ eps: # (0.000, 2.664)
```

```
        eqFile.write("%d) x1, y1, z1 is (%.4f, %.4f, %.4f)
                \n" %(II, x1, y1, z1))

        ra.ReferencePoint(point
                = (x1, y1, 0.0)) #Create reference points at Q and S edges
        # # # select vertical node set
        if x1 ≥ −0.1 * eps and x1 ≤ a + 0.1 * eps:
# Resin mesh distance 0.074 mm &(0.00, 2.664) next line bounding boxes
are small boxes to get the vertical set of nodes
          box1 = n.getByBoundingBox(−0.5 * (0.074) + x1, −1.0 * (eps)
                + y1, −1.0 * (eps) − (maxtowheight * 2) + z1, x1 + 0.5
                * (0.074), y1 + 1.0 * (eps), eps + (maxtowheight * 2) + z1)
        if y1 < 0.1 and x1 < 2.665: #(0.000, 2.664)
          #Create node set S
          name1 = 'S_1_L_%d'%S1count
          ra.Set(name = name1, nodes = box1)
          RPn = (ra.referencePoints.findAt((x1, y1,0.0)),)
          refNodename = 'RP_S_1_%d'%S1count
          ra.Set(referencePoints = RPn, name = refNodename)

          #Create dummy nodes
          ra.ReferencePoint(point = (x1, y1 − 0.2,0.0))
          RPn = (ra.referencePoints.findAt((x1, y1 − 0.2,0.0)),)
          eqFile1.write("%d) QS1_%d  x1, y1, z1 is (%.4f, %.4f, %.4f)
                \n" %(II, Q1count, x1, y1, z1))
          refNodename = 'NODE_X1_%d'%S1count
          ra.Set(referencePoints = RPn, name = refNodename)

          #apply MPCs along vertical nodes on each tow boundry
          region1 = ra.sets['RP_S_1_%d'%S1count]
          region2 = ra.sets['S_1_L_%d'%S1count]
          Model.MultipointConstraint(name = 'MPC_S_1_L_%d'%S1count,
          controlPoint = region1, surface = region2, mpcType = BEAM_MPC,
          userMode = DOF_MODE_MPC, userType = 0, csys = None)

          RefPoint_X1[S1count − 1] = x1
          S1count = S1count + 1

        elif y1 > 2.66 and x1 < 2.665:
# y vlues of adjacent nodes to the edge nodes 0.042,2.62
          #Create node set Q
          name1 = 'Q_1_L_%d'%Q1count
          ra.Set(name = name1, nodes = box1)
          RPn = (ra.referencePoints.findAt((x1, y1,0.0)),)
          #eqFile1.write("%d) QS1_%d  x1, y1, z1 is (%.4f, %.4f, %.4f)
                \n" %(II, Q1count, x1, y1, z1))
```

```
        refNodename = 'RP_Q_1_%d'%Q1count
        ra.Set(referencePoints = RPn, name = refNodename)

        #apply MPCs along vertical nodes on each tow boundry
        region1 = ra.sets['RP_Q_1_%d'%Q1count]
        region2 = ra.sets['Q_1_L_%d'%Q1count]
        Model.MultipointConstraint(name = 'MPC_Q_1_L_%d'%Q1count,
        controlPoint = region1, surface = region2, mpcType = BEAM_MPC,
        userMode = DOF_MODE_MPC, userType = 0, csys = None)
        Q1count = Q1count + 1

#Create reference points at P and R edges
if z1 < 1 * eps and z1 >= -1 * eps: ##(0.00)
  if x1 <= 0.0 + 0.2 * eps or x1 >= a - 0.1 * eps: #(0.00, 2.664)
    eqFile.write("%d) x1, y1, z1 is (%.4f, %.4f, %.4f)
            \n" %(II, x1, y1, z1))

    ra.ReferencePoint(point
            = (x1, y1, 0.0)) #Create reference points at P and R edges
    #select vertical node set
    if (y1 >= 0.0 - 0.1 * eps and y1 <= b + 0.1 * eps) :
      box1 = n.getByBoundingBox(-1.0 * eps + x1, -0.5 * 0.074
            + y1, -1.0 * eps - (maxtowheight * 2.0) + z1, eps + x1,0.5
            * 0.074 + y1,1.0 * eps + (maxtowheight * 2.0) + z1)
    if x1 < 0.1 and y1 < 2.665:
      #Create node set
      name1 = 'P_1_L_%d'%P1count
      ra.Set(name = name1, nodes = box1)
      RPn = (ra.referencePoints.findAt((x1, y1,0.0)),)
      eqFile1.write("%d) RP1_%d x1, y1, z1 is (%.4f, %.4f, %.4f)
            \n" %(II, P1count, x1, y1, z1))
      refNodename = 'RP_P_1_%d'%P1count
      ra.Set(referencePoints = RPn, name = refNodename)

      #Create dummy nodes
      ra.ReferencePoint(point = (x1 - 0.2, y1,0.0))
      RPn = (ra.referencePoints.findAt((x1 - 0.2, y1,0.0)),)
      refNodename = 'NODE_Y1_%d'%P1count
      ra.Set(referencePoints = RPn, name = refNodename)

      #apply MPCs along vertical nodes on each tow boundry
      region1 = ra.sets['RP_P_1_%d'%P1count]
      region2 = ra.sets['P_1_L_%d' %P1count]
      Model.MultipointConstraint(name = 'MPC_P_1_L_%d'%P1count,
      controlPoint = region1, surface = region2, mpcType = BEAM_MPC,
      userMode = DOF_MODE_MPC, userType = 0, csys = None)
```

```
        RefPoint_Y1[P1count − 1] = y1
        P1count = P1count + 1


    elif x1 > 2.66 and y1 < 2.665:
        #Create node set
        name1 = 'R_1_L_%d'%R1count
        ra.Set(name = name1, nodes = box1)
        RPn = (ra.referencePoints.findAt((x1, y1,0.0)),)
        refNodename = 'RP_R_1_%d'%R1count
        ra.Set(referencePoints = RPn, name = refNodename)

        #apply MPCs along vertical nodes on each tow boundry
        region1 = ra.sets['RP_R_1_%d'%R1count]
        region2 = ra.sets['R_1_L_%d' %R1count]
        Model.MultipointConstraint(name = 'MPC_R_1_L_%d'%R1count,
        controlPoint = region1, surface = region2, mpcType = BEAM_MPC,
        userMode = DOF_MODE_MPC, userType = 0, csys = None)

        R1count = R1count + 1


#apply Equations constrains for PBCs
for I in range(3,38):
    #DOF1
    Model.Equation(name = 'EQdof1 − SQ − 1 − %d'%I, terms
= ((1.0,'RP_S_1_%d'%I, 1), (−1.0,'RP_Q_1_%d'%I, 1), (−2.664,'NODE_X1_%d'%I, 1)))
    Model.Equation(name = 'EQdof1 − PR − 1 − %d'%I, terms
= ((1.0,'RP_R_1_%d'%I, 1), (−1.0,'RP_P_1_%d'%I, 1), (−2.664,'NODE_Y1_%d'%I, 1)))

    #DOF2
    Model.Equation(name = 'EQdof2 − SQ − 1 − %d'%I, terms
= ((1.0,'RP_S_1_%d'%I, 2), (−1.0,'RP_Q_1_%d'%I, 2), (−2.664,'NODE_X1_%d'%I, 2)))
    Model.Equation(name = 'EQdof2 − PR − 1 − %d'%I, terms
= ((1.0,'RP_R_1_%d'%I, 2), (−1.0,'RP_P_1_%d'%I, 2), (−2.664,'NODE_Y1_%d'%I, 2)))

    #DOF3
    Model.Equation(name = 'EQdof3 − SQ − 1 − %d'%I, terms
                = ((1.0,'RP_S_1_%d'%I, 3), (−1.0,'RP_Q_1_%d'%I, 3), ((2.664
                * RefPoint_X1[I − 1]),'NODE_X1_%d'%I, 3)))
    Model.Equation(name = 'EQdof3 − PR − 1 − %d'%I, terms
                = ((1.0,'RP_R_1_%d'%I, 3), (−1.0,'RP_P_1_%d'%I, 3), ((2.664
                * RefPoint_Y1[I − 1]),'NODE_Y1_%d'%I, 3)))

    #DOF4
```

$$Model.Equation(name = 'EQdof4 - SQ - 1 - \%d'\%I, terms = ((1.0, 'RP\_S\_1\_\%d'\%I, 4), (-1.0, 'RP\_Q\_1\_\%d'\%I, 4), (2.664, 'NODE\_X1\_\%d'\%I, 4)))$$

$$Model.Equation(name = 'EQdof4 - PR - 1 - \%d'\%I, terms = ((1.0, 'RP\_R\_1\_\%d'\%I, 4), (-1.0, 'RP\_P\_1\_\%d'\%I, 4), (2.664, 'NODE\_Y1\_\%d'\%I, 4)))$$

$$\#DOF5$$

$$Model.Equation(name = 'EQdof5 - SQ - 1 - \%d'\%I, terms = ((1.0, 'RP\_S\_1\_\%d'\%I, 5), (-1.0, 'RP\_Q\_1\_\%d'\%I, 5), (-2.664, 'NODE\_X1\_\%d'\%I, 5)))$$

$$Model.Equation(name = 'EQdof5 - PR - 1 - \%d'\%I, terms = ((1.0, 'RP\_R\_1\_\%d'\%I, 5), (-1.0, 'RP\_P\_1\_\%d'\%I, 5), (-2.664, 'NODE\_Y1\_\%d'\%I, 5)))$$

$$\#DOF6$$

$$Model.Equation(name = 'EQdof6 - SQ - 1 - \%d'\%I, terms = ((1.0, 'RP\_S\_1\_\%d'\%I, 6), (-1.0, 'RP\_Q\_1\_\%d'\%I, 6), (0, 'NODE\_X1\_\%d'\%I, 6)))$$

$$Model.Equation(name = 'EQdof6 - PR - 1 - \%d'\%I, terms = ((1.0, 'RP\_R\_1\_\%d'\%I, 6), (-1.0, 'RP\_P\_1\_\%d'\%I, 6), (0, 'NODE\_Y1\_\%d'\%I, 6)))$$

$$eqFile1.close()$$

Appendix C: MATLAB code used to calculate the ABD matrix of Resin embedded model

```
%l= length of the unit cell
l=2.664;
vf=[];%virtual force matrix
vd=[]; %virtual displacement matrix
conv_R=[1 0 0 0 0 0;0 1 0 0 0 0;0 0 −1 0 0 0;0 0 0 −1 0 0;0 0 0 0 1 0;0 0 0 0 0 1];
conv_P=[−1 0 0 0 0 0;0 −1 0 0 0 0;0 0 −1 0 0 0;0 0 0 −1 0 0;0 0 0 0 −1 0;0 0 0 0 0
−1];

eq_S1Q1 = [0.0740 0.1480 0.2220 0.2960 0.3700 0.4440 0.5180 0.5920 0.6660
 0.7400 0.8140 0.8880 0.9620 1.0360 1.1100 1.1840 1.2580 1.3320 ];

eq_S2Q2 = [1.4060 1.4800 1.5540 1.6280 1.7020 1.7760 1.8500 1.9240 1.9980
2.0720 2.1460 2.2200 2.2940 2.3680 2.4420 2.5160 2.5900 ];

eq_P1R1 = [0.0740 0.1480 0.2220 0.2960 0.3700 0.4440 0.5180 0.5920 0.6660
0.7400 0.8140 0.8880 0.9620 1.0360 1.1100 1.1840 1.2580 1.3320];

eq_P2R2 = [1.4060 1.4800 1.5540 1.6280 1.7020 1.7760 1.8500 1.9240 1.9980
2.0720 2.1460 2.2200 2.2940 2.3680 2.4420 2.5160 2.5900];

% T=[t1,t2,t3,t4];
for file=1:6
   filenumber=int2str(file);
   filename=['Test_',filenumber,'.txt'];
   %read outputs from the text files
   [a1,b1,c1,d1,e1,f1,g1,h1,i1,j1,k1,l1]=textread(filename,'%s %s %s %s %s
%s %s %s %s %s %s %s',1057);
   data=[b1 c1 d1 e1 f1 g1];
   impo=data;
   R1=[];
% Matrix for reaction value storage 6 forces R1,R2,Q1,Q2 (column matrix)
   P1=[];
 % Matrix for reaction value storage 6 forces P1,P2,S1,S2 (column matrix)
   bb=[]; % Keeping 48 reaction forces (column matrix)
   X1=[];
   i=1;
   p=5;
   g=1;
```

```
while p<354
% number of the last line of the resultant force in the text file +1
    i = ceil(p/18);
    t1=[1/2.664 0 0 0 0 0;0 0.5/1.332 0 0 0 0;0 0 1/(2.664*eq_P1R1(1,i)) 0 0 0;0 0 0
0.5/1.332 0 0;0 0 0 0 1/2.664 0;0 0 0 0 0 1];
    t2=[1/2.664 0 0 0 0 0;0 0.5/1.332 0 0 0 0;0 0 1/(2.664*eq_P2R2(1,i)) 0 0 0;0 0 0
0.5/1.332 0 0;0 0 0 0 1/2.664 0;0 0 0 0 0 1];
    t3=[0.5/1.332 0 0 0 0 0;0 1/2.664 0 0 0 0;0 0 1/(2.664*eq_S1Q1(1,i)) 0 0 0;0 0 0
1/2.664 0 0;0 0 0 0 0.5/1.332 0;0 0 0 0 0 1];
    t4=[0.5/1.332 0 0 0 0 0;0 1/2.664 0 0 0 0;0 0 1/(2.664*eq_S2Q2(1,i)) 0 0 0;0 0 0
1/2.664 0 0;0 0 0 0 0.5/1.332 0;0 0 0 0 0 1];

    R1(:,1)=str2double(data(p,:));
    R1=conv_R*R1;
    if rem(g,4)==1
       X1=t1*R1;
    elseif rem(g,4)==2
       X1=t2*R1;
    elseif rem(g,4)==3
       X1=t3*R1;
    elseif rem(g,4)==0
       X1=t4*R1;
    end

    bb=[bb;X1];

    P1=conv_P*R1;
     if rem(g,4)==1
       P1=t1*P1;
    elseif rem(g,4)==2
       P1=t2*P1;
    elseif rem(g,4)==3
       P1=t3*P1;
    elseif rem(g,4)==0
       P1=t4*P1;
    end
    bb=[bb;P1];

    p=p+4;
    g=g+1;
```

```
    i=i+1;
  end

  vf=[vf bb]; %Virtual Force Matrix
  UR=[]; %Virtual Displacemnts U1,U2,U3,UR1,UR2,UR3
  cc=[]; %Keeping 48 Displacemet values
  t=357; % starting line number of resultant displacement
  while t<1058 % length of the data variable +1
    UR(:,1)=str2double(data(t,:));
    cc=[cc;UR];
    t=t+4;
  end
  vd=[vd cc];
  D=1/7.096896;
  Matrix=transpose(vd)*vf;
  ABD_Matrixi=D*Matrix;
end
ABD_Matrixi
```

Appendix D: ABD matrices of fibre in-phase, 90° phase shift, and fibre out-of-phase RUC models.

$$ABD_{0°\ phase\ shift} = \begin{pmatrix} 8503.8 & 2132.1 & 0 & 7 & 2 & 2 \\ 2132.1 & 8526.3 & 0 & 2 & 7 & 2 \\ 0 & 0 & 312.6 & 0 & 0 & 0 \\ 7 & 2 & 0 & 36.4 & 4.4 & 0 \\ 2 & 7 & 0 & 4.4 & 36.4 & 0 \\ 5 & 5 & 0 & 0 & 0 & 1.6 \end{pmatrix}$$

$$ABD_{90°phase\ shift} = \begin{pmatrix} 10076.3 & 914.5 & +0.1 & +9.2 & -4.2 & 0 \\ 914.6 & 10074.1 & 0 & -4.8 & +7.2 & 0 \\ +0.1 & 0 & 316.8 & 0 & 0 & +1.3 \\ +9.2 & -4.7 & 0 & 35.2 & +4.5 & 0 \\ -4.2 & +7.2 & 0 & +4.5 & 34.9 & 0 \\ 0 & 0 & +1.3 & 0 & 0 & +1.7 \end{pmatrix}$$

$$ABD_{180°phase\ shift} = \begin{pmatrix} 9506.6 & 1226.2 & +1 & -3 & 0 & 0 \\ 1226.3 & 9553.0 & 0 & 0 & +3 & 0 \\ -3 & +1 & 312.6 & 0 & 0 & 0 \\ 0 & +1 & 0 & 38.5 & +9.2 & 0 \\ +1 & 0 & 0 & +9.2 & 38.8 & 0 \\ 0 & 0 & 0 & 0 & 0 & +1.8 \end{pmatrix}$$